Title:

Interaction of GAT1 with sodium ions: from efficient recruitment to stabilisation of substrate and conformation

Authors:

Erika Lazzarin[1$], Ralph Gradisch[1$], Sophie M.C. Skopec[1], Leticia Alves da Silva[1], Dániel Szöllősi[1,2], Julian Maier[1], Sonja Sucic[1], Baruch I. Kanner[3], Harald H. Sitte[1,4,5], Thomas Stockner[1#]

Affiliations:

[1] Centre for Physiology and Pharmacology, Institute of Pharmacology, Medical University of Vienna, Waehrigerstr. 13A, 1090 Vienna, Austria

[2] Department of Theoretical and Computational Biophysics, Max Planck Institute for Multidisciplinary Sciences, Am Fassberg 11, 37077 Göttingen, Germany

[3] Department of Biochemistry and Molecular Biology, Institute for Medical Research Israel-Canada, Hebrew University, Hadassah Medical School, Jerusalem 91120, Israel

[4] Hourani Center for Applied Scientific Research, Al-Ahliyya Amman University, Amman, Jordan

[5] Center for Addiction Research and Science-AddRess, Medical University Vienna, Waehringer Strasse 13A, 1090, Vienna, Austria

#corresponding author

Thomas Stockner; email: thomas.stockner@meduniwien.ac.at

$ Shared first authors

These authors contributed evenly to the manuscript.

Keywords:

GAT1, GABA, transporter, sodium binding, recruiting site

Abstract

The human GABA transporter (GAT1) is a membrane transporter that mediates the reuptake of the neurotransmitter GABA from the synaptic cleft into neurons and glial cells. Dysregulation of the transport cycle has been associated with epilepsy and neuropsychiatric disorders, highlighting the crucial role of the transporter in maintaining homeostasis of brain GABA levels. GAT1 is a secondary active transporter that couples the movement of substrate to the simultaneous transport of sodium and chloride ions along their electrochemical gradients. Using MD simulations, we identified a novel sodium recruiting site at the entrance to the outer vestibule, which attracts positively charged ions and increases the local sodium concentration, thereby indirectly increasing sodium affinity. Mutations of negatively charged residues at the recruiting site slowed the binding kinetics, while experimental data revealed a change in sodium dependency of GABA uptake and a reduction of sodium affinity. Simulation showed that sodium displays a higher affinity for the sodium binding site NA2, which plays a role in the stabilisation of the outward-open conformation. We directly show that the presence of a sodium ion bound to NA2 increases the stability of the closed inner gate and restrains motions of TM5. We find that sodium is only weakly bound to NA1 in the absence of GABA, while the presence of the substrate strengthens the interaction due to the completed ion coordinating shell, explaining cooperativity of between GABA and sodium.

Introduction

γ-aminobutyric acid (GABA) is the main inhibitory neurotransmitter in the central nervous system (CNS) (Krnjević and Schwartz, 1967). Release of GABA from the presynaptic neuron into the synaptic cleft triggers hyperpolarization of the postsynaptic neuron through activation of $GABA_A$ receptors (Ghit et al., 2021). GABA is removed from the synaptic cleft by several GABA transporters, namely GAT1, GAT2, GAT3 and the betaine/GABA transporter BGT1. These are sodium- and chloride- dependent secondary active transporters from the SLC6 family (Bhatt et al., 2023; Kanner, 1978; Kristensen et al., 2011) and GAT1 is the first cloned member of the family (Guastella et al., 1990). Within the GABA transporter family, the presynaptic GAT1 is the main neuronal GABA uptake transporter. Dysregulation of GAT1 function has been associated with epilepsy and neuropsychiatric disorders (Fischer et al., 2022; Kasture et al., 2023), highlighting the crucial role of GAT1 in maintaining neurotransmitter homeostasis in the brain (Bhat et al., 2021; Schousboe et al., 2004; Schousboe and Madsen, 2017)

GAT1 consists of 12 transmembrane helices (TM) (Motiwala et al., 2022) and shares the pseudo-symmetric inverted repeat motif (Forrest et al., 2008) of the “LeuT fold” with the other SLC6 family members, including the fold defining bacterial small amino acid transporter LeuT (Yamashita et al., 2005), the Drosophila dopamine transporter dDAT (Penmatsa et al., 2013), and the human serotonin transporter hSERT (Coleman et al., 2016), which was the first structure for a human transporter of the SLC6 family. TM3, 4, 5, 8 and 9 constitute the core of the rigid scaffold domain, while TM1, 2, 6 and 7 assemble into the more mobile bundle domain. The motion of the bundle domain relative to the scaffold domain allows for alternating access to the central substrate binding site S1 (Forrest et al., 2008).

Very recently, several inward-facing GAT1 structures and a substrate, sodium and chloride-bound inward-occluded structure were published (Motiwala et al., 2022; Nayak et al., 2023). These conformations together with an AlphaFold2 model of the outward-facing state have

allowed to formulate the translocation cycle for GAT1 (Nayak et al., 2023; Zhu et al., 2023) which consists of outward-open, occluded and inward-open states. Interestingly, while the conformations of the outward-open and the occluded structures are very similar to the respective conformations observed in other SLC6 family members (Coleman et al., 2016; Singh et al., 2008; Yamashita et al., 2005; Yang and Gouaux, 2021), confirming shared structural changes across the SLC6 family, SLC6 transporter structures differ in the conformation of TM1a of the inward-facing state, whereby for GAT1 several conformations of TM1a were observed (Motiwala et al., 2022; Nayak et al., 2023; Zhu et al., 2023). For LeuT we have shown that the large motions of TM1a as observed in the micelle solubilized crystal structure (doi: 10.1038/nature10737) are incompatible within the membrane environment (Sohail et al., 2016), suggesting that the conformation of TM1a is especially sensitive to the environment.

The concentrative uptake of GABA is enabled by the co-transport with two sodium ions and one chloride (Bhatt et al., 2023; Hilgemann and Lu, 1999; Keynan and Kanner, 1988). The chloride binding site and the two sodium binding sites (NA1 and NA2) are located in the centre of the transporter, next to the unwound regions on TM1 and TM6, which form the substrate binding site (S1) together with TM3 and TM8 (Nayak et al., 2023; Zhu et al., 2023; Zomot et al., 2007). Structural considerations on LeuT (Krishnamurthy and Gouaux, 2012; Yamashita et al., 2005) and biochemical studies (Tavoulari et al., 2016) indicate that the sodium bound to the NA2 (Na2) is involved in stabilisation of the outward-open state by connecting TM1 of the bundle with TM8 of the scaffold. The sodium ion bound to the NA1 (Na1) is exclusively interacting with the bundle domain. It stabilises the bound substrate by directly interacting with its carboxyl group in GAT1 and LeuT.
Here we present direct evidence for the mechanism by which the two sodium ions exert their function in GAT1. Using a set of 60 simulations starting from the sodium-free outward-open GAT1 state, we investigated sodium binding to and the response of GAT1 to the presence of sodium ions. We observed comparable probability for initial binding of sodium to either NA1 or NA2. Importantly, only Na2 was stably bound, while we observed several unbinding events of Na1 from NA1 and in some cases a transfer of the sodium to NA2. Analysis of the simulations identified a clear sodium entry path with a sodium recruiting site at the entry to the extracellular vestibule and revealed a temporary site in the S1. The role of the recruiting site that includes two negatively charged residues (D281 and E283) on TM6a is to attract sodium ions, which increases the local sodium concentration and accelerates sodium binding. We find that Na1 stabilises GABA in the S1 by including its carboxyl moiety into the first interaction shell of Na1, holding the carboxyl moiety in the same position is space as the carboxylate of the conserved aspartate (D98 in SERT, D79 in DAT) of the monoamine transporters. Na2 is directly linked to the mobility of the bundle domain as Na2 binding reduces its mobility as well as increases the stability of the inner gate between TM1, TM5 and TM6.

Results

The path taken by sodium to reach NA1 and NA2

Sodium ions reach the ion binding sites NA1 and NA2 through the outer vestibule. Binding to the outward-open conformation of SLC6 transporters is a fast process in the nano to microsecond time range (Bicho and Grewer, 2005; Hasenhuetl et al., 2016; Hilgemann and Lu, 1999; Szöllősi and Stockner, 2021), therefore allowing for an unbiased direct simulation approach. Using 60 independent simulations, we repeatedly observed that sodium ions spontaneously entered the outward-open vestibule of GAT1. To characterise the path that sodium ions take for reaching the S1 and for binding to NA1 and NA2, we derived an averaged sodium density with a 0.1 nm spatial resolution from the sodium positions observed in all simulations. These sodium density maps (Figure 1a, b) highlight the regions with a high probability of observing sodium ions. The density analysis shows that sodium ions initially accumulate at the rim of the outer vestibule. This sodium recruitment site comprises two negatively charged amino acids (D281 and E283) that are located at the beginning of TM6 (Figure 1a). The high sodium density at the recruitment site shows that sodium can more likely be found at the recruiting site compared to the extracellular solution. This locally higher concentration increases the probability of binding, because sodium ions can leave the recruitment site in two directions: either (i) enter the open outer vestibule towards the S1, attracted by the negative field in the S1 and the outer vestibule, or (ii) detach from GAT1 and diffuse into the external solution.

The salt bridge of the extracellular gate between R69 and D451 was defined as the structural threshold for considering a sodium ion within the vestibule, because once beyond this gate, ions would typically not leave the vestibule, but reach the S1 and bind to NA1 or NA2. We independently analysed trajectories in which sodium would bind to the NA1 or NA2 and found that the routes sodium ions take through the outer vestibule are indistinguishable. Once in the S1, sodium ions immediately bound to NA1 or NA2, or reside for some time in a temporary pre-binding site within the S1 and only in a second step reach NA1 or NA2 (Figure 1d-f). In some cases, Na1 unbound from the NA1 returning to this temporary site, and occasionally bound to NA2 in a second step. We did not observe unbinding from the NA2. This temporary pre-binding site (Figure 1b) for sodium overlaps with the region where the positively charged amino group of the substrate GABA resides in the ligand-bound conformation (Zhu et al., 2023). A similar temporary site and comparable binding kinetics were observed in simulations of direct sodium binding to SERT (Szöllősi and Stockner, 2021). It also overlaps with the region where the positively charged amino group of serotonin was found in SERT (Gradisch et al., 2022; Yang and Gouaux, 2021) suggesting that the temporary binding site is a common feature of SLC6 transporters.

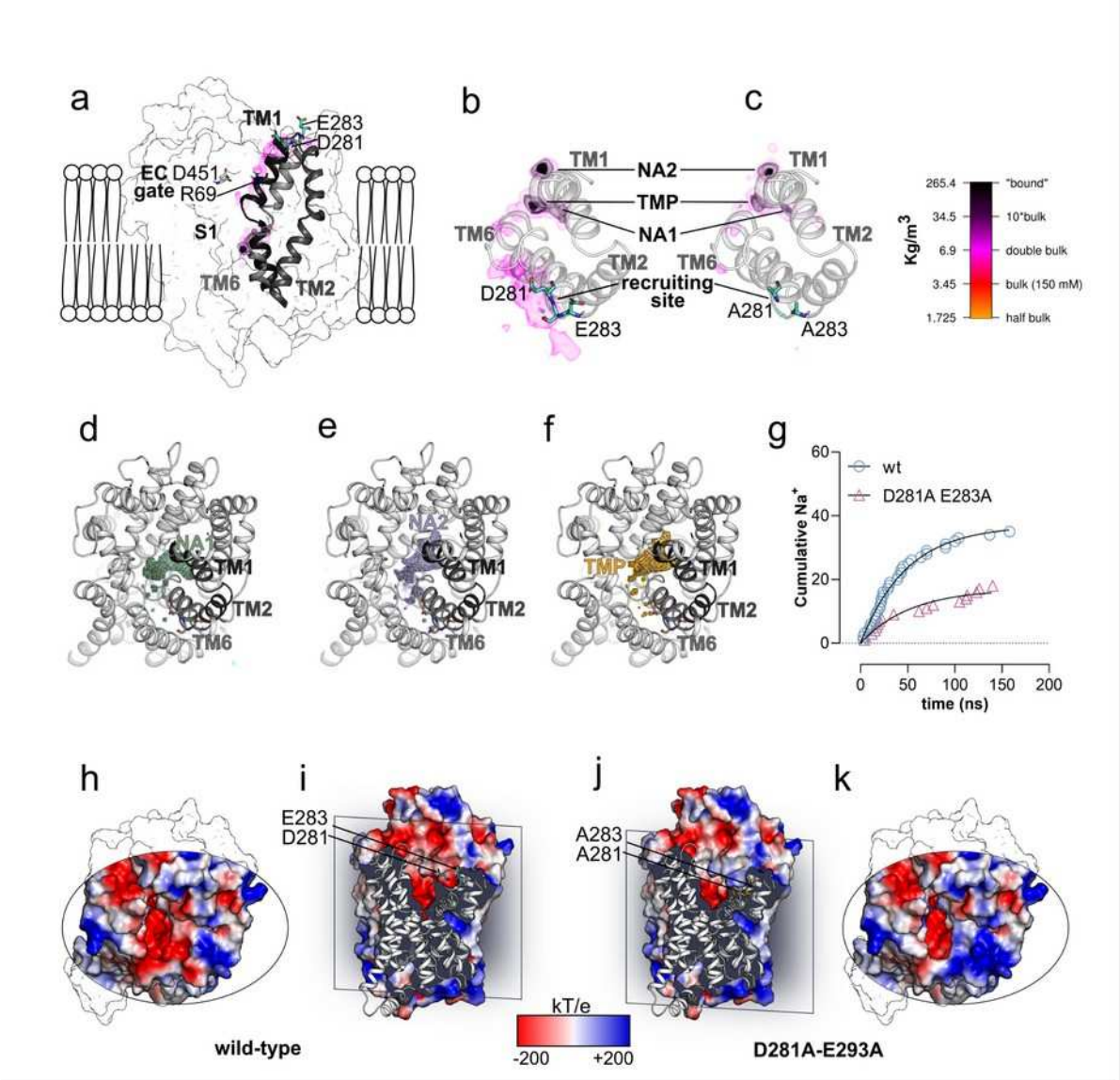

Figure 1: Sodium binding and GAT1 electrostatics ***a****) Averaged density of sodium is shown in close proximity to GAT1 in a side view. The GAT1 surface is shown in white, the transmembrane helices TM1, TM2, and TM6 are highlighted in grey. The residues (*R69 and D451*) forming the salt bridge of the extracellular gate (EC gate) are shown as grey sticks, the recruiting site residues D281 and E283 as cyan sticks. The sodium density is represented as isovolume and coloured according to the legend in panel c. The trajectories were fitted to the Cα atoms of the transmembrane domain* ***b)*** *Top view of GAT1, showing TM1, TM2 and TM6, the regions of high density of sodium and the recruiting site residues, coloured according to the legend in panel c. Sodium density at the temporary site is indicated by TMP.* ***c)*** *Same as in panel b, but data are from the double alanine (D281A and E283A) mutant simulations. The scale bar to the right explains the colour code of sodium density.* ***d)*** *Positions of sodium ions binding directly to NA1 (green),* ***e)*** *directly NA2 in purple or* ***f)*** *first residing in the temporary binding site (orange) before reaching NA1 or NA2.* ***g)*** *Quantification of sodium binding events, calculated as cumulative sodium ions entering the vestibule.* ***h)*** *Top view and* ***i)*** *side view of the electrostatic potential of GAT1 wild-type mapped onto its surface.* ***j)*** *Top and* ***k)*** *side view of the electrostatic potential of the double alanine mutant (D281A and E283A).*

Role of the sodium recruitment site

Sodium ions consistently interact first with the recruiting site at the beginning of the outer vestibule before passing through the outer vestibule and binding to NA1 or NA2. Although negatively charged residues are present in other regions of the extracellular vestibule, and alternative pathways for sodium entry are available, sodium preferentially follows the same path, presumably, because attracted to the recruiting site. Electrostatic potentials (Figure 1h,i) showed the expected strong negative potential in the S1 and the vestibule, but also revealed a strong negative potential at the recruitment site. The residues D281 and E283 are in the centre of this area of negative electrostatic potential. Corresponding negatively charged residues were identified in several other SLC6 transporters, and their mutation in the paralog transporters DAT and SERT were shown to reduce substrate transport or sodium binding (Chen et al., 2004; Kortagere et al., 2013; Szöllősi and Stockner, 2021). *In silico* neutralisation of these charges by alanine mutations (D281A-E283A) collapsed the local negative electrostatic potential, as it changed sign and became weekly positive (Figure 1j,k), supporting the notion of an electrostatic attraction. To explore the impact of D281 and E283 on sodium binding, the double alanine mutation (D281A-E283A) was introduced in GAT1 wild-type and ion binding simulations were repeated from the same 60 systems. Consistent with the inference from the electrostatic potential, the density analysis showed a strongly reduced sodium density at the recruitment site (Figure 1c), confirming that sodium ions are electrostatically attracted and that residues D281 and E283 play a critical role. The overall sodium density in the S1, NA1 and NA2 was also lower due to the slower binding kinetics leading to a lower number of sodium binding events.

To determine the importance of the recruitment site for sodium binding, we quantified the kinetics of sodium entering the S1. Figure 1g shows the time dependent cumulative number of simulations in which a sodium ion enters the S1. The data (Figure 1g) revealed that the double mutant reduced the binding kinetics as compared to wild-type GAT1, thereby showing that the recruitment site accelerates the rate of sodium binding.

To verify this prediction in vitro, we mutated D281 and E283 to alanine and stably expressed the double mutant in HEK293 cells to experimentally measure uptake and transport associated currents of wild-type GAT1 and of the D281A-E283A variant. The GAT1 double mutant showed 4-fold smaller surface expression as compared to wild-type (Figure 2a,b), but plasma membrane localisation was clearly detectable, as visible in the insert of Figure 2a. We quantified membrane expression of the YFP tagged GAT1 by measuring the mean fluorescence of intracellular and membrane localised GAT1 (Figure 2b). The cytosolic fluorescence was similar for wild-type and the D281A-E283A variant, while the surface expression of wild-type was 4 fold higher. To verify functional expression of the D281A-E283A variant of GAT1, we measured dose-dependent GABA uptake (Figure 2c). Consistent with surface expression, uptake of GABA was 4 fold lower in the D281A-E283A double mutant (Figure 2c,d), while Km was only two fold lower (wild-type GAT1 (Km: 12.41 ± 4.32 μM), double mutant (Km: 5.99 ± 2.86 μM). To functionally characterise the D281A-E283A variant of GAT1, we measured transport function using electrophysiological recordings, as GABA transport by GAT1 is electrogenic. Representative traces of GABA uptake dependent currents are shown for wild type GAT1 (Figure 3a) and the D281A-E283A double mutant (Figure 3c). The concentration-response of GABA uptake showed for wild-type GAT1 (Figure 3b) an EC50 of 18.60 μM [confidence interval: 33.40 μM, 44.23 μM]. The EC50 for the D281A-E283A variant is similar (Figure 3d), confirming that the double mutant

affected expression, but not the intrinsic transport function of GAT1 at physiological conditions (Figure 3e). Simulations suggested that the double mutant (D281A-E283A) would affect sodium binding. To unmask a possible effect of sodium on GABA transport, we carried out GABA uptake with increasing concentrations of transport energising sodium. The results (Figure 3f, g) showed that the D281A-E283A double mutant changed the sodium dependency of GABA transport: while the EC50 wild-type GAT1 is 46.05 ± 4.55 µM, the EC50 of the D281A-E283A variant is increased to 80.73 ± 14.28 µM. The observed shift of the dose response curve to the right showed that the Km of sodium dependency of GABA transport is reduced by approximately 57%, verifying the computational predictions that D281 and E283 at the recruitment site effectively increase the local concentration of sodium at the entry to the outer vestibule which leads to a locally increased sodium concentration and an enhanced sodium binding

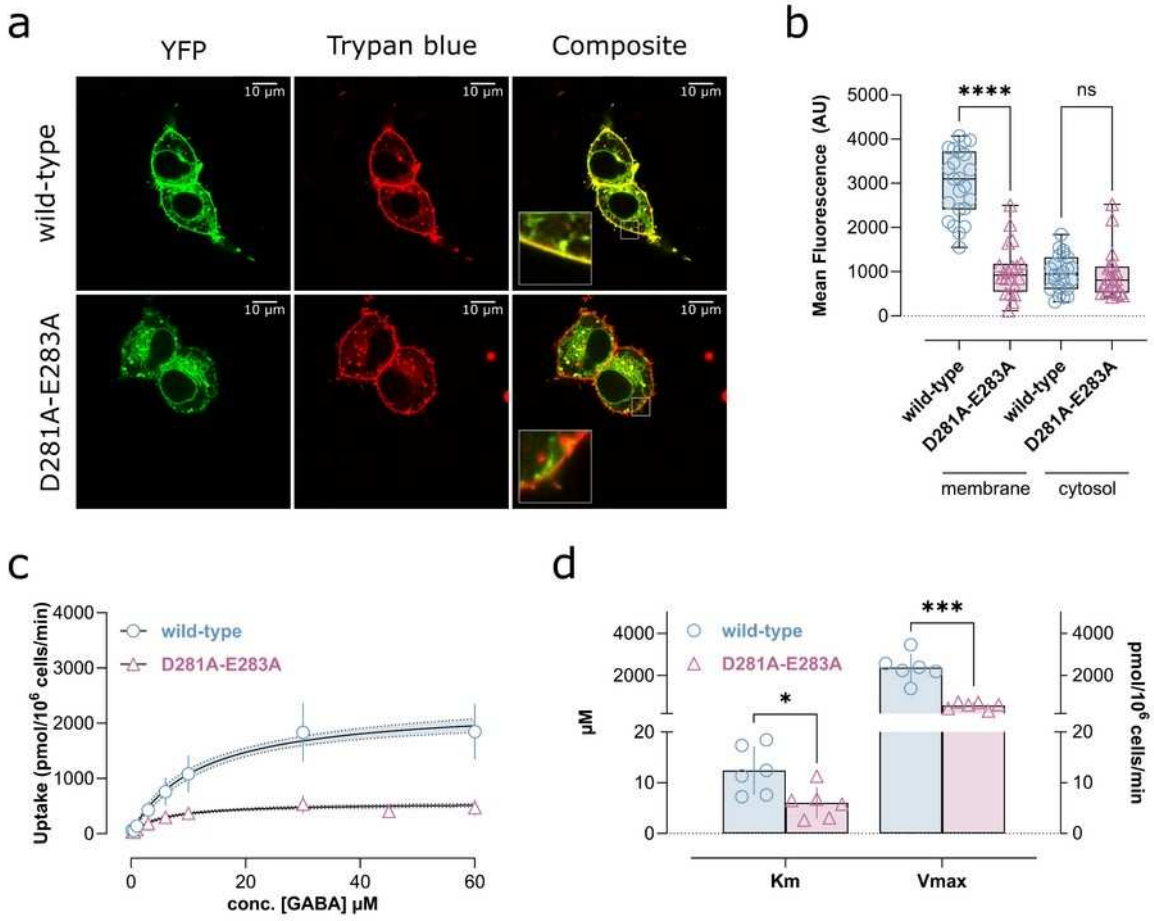

***Figure 2. Effect of D281A-E283A mutation**: **a)** Representative confocal microscopy images of GAT1 wild-type and double alanine mutant (D281A-E283A) expressed in HEK293 cells. Transporters were N-terminally tagged with YFP, the cell membrane was stained by trypan blue. Composite images display the superimposition of tagged GAT1 and trypan blue stained membranes. The inserts in the lower left corner show a zoom-in on the cell membrane. **b)** Mean fluorescence of cytosolic and membrane resident YFP tagged GAT1. **c)** Concentration-dependent [^{3}H]GABA uptake in HEK293 cells stably expressing GAT1*

wild-type and D281A-E283A. ***d)*** *Quantification of the Km (µM) and the Vmax (pmol/10^6 cells/min) of the GABA uptake. Data is displayed as mean ± SD. Concentration dependent uptake was measured in triplicates in six biologically independent experiments. Single data points for Km and Vmax are the averages for individual experiments.*

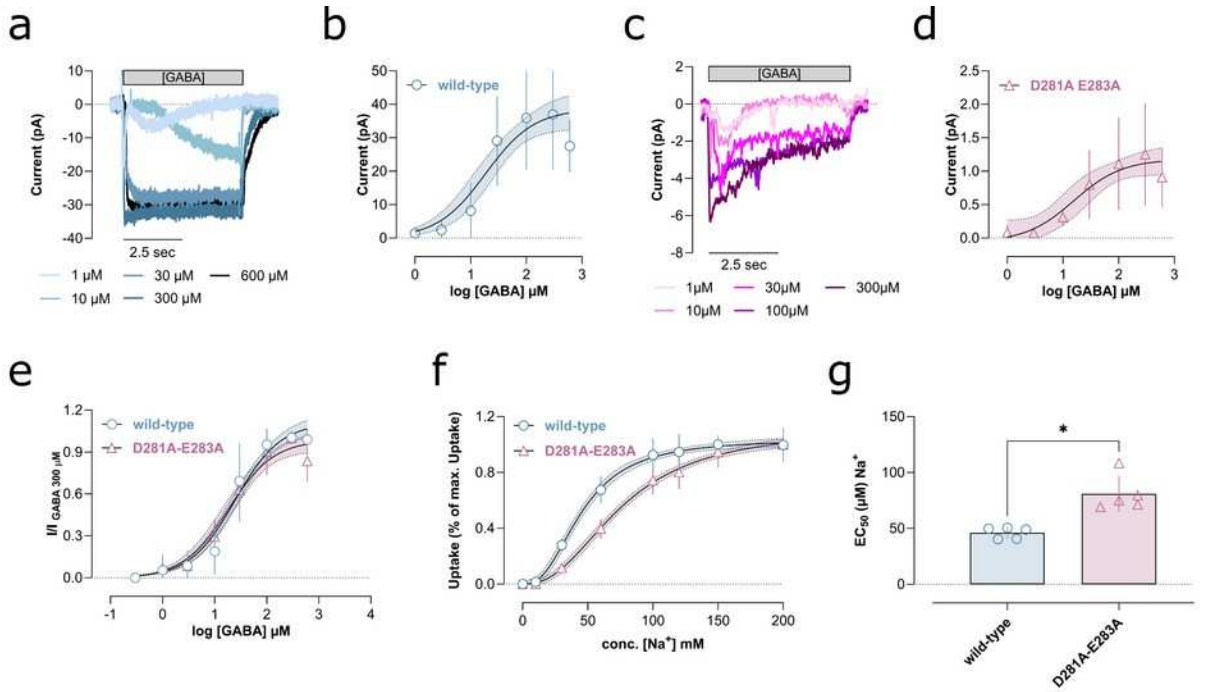

Figure 3. Effect of D281A-E283A mutation*: **a)** Representative traces of whole-cell patch clamp recordings showing GAT1 wild-type mediated currents in response to different GABA concentrations. **b)** Concentration dependent average steady state currents. **c)** Representative traces of whole-cell patch clamp experiments showing concentration-dependent GAT1 D281A-E283A mediated currents (data points are shown as running average (n=11) traces). **d)** Average steady state currents plotted against the used GABA concentration. **e)** Comparison of concentration dependent average steady state currents of GAT1 wild-type and double mutant, normalised to the respective currents observed at 300 µM GABA. **f)** Normalised sodium-dependent [^{3}H]GABA uptake curve. **g)** Sodium EC_{50} values for GAT1 wild-type and the double mutant D281A-E283A observed in panel f. Data is shown as mean ± SD from 5 biological independent replicas of [^{3}H]GABA uptake experiments measured in triplicates. In case of electrophysiological measurements, at least 7 independent recordings from 7 independent cells were recorded.*

Local structural changes in the sodium binding sites NA1 and NA2

Binding of ligands is frequently accompanied by structural changes in the protein, both in the immediate vicinity of the binding site and at distant locations. Conformational selection and induced fit are two models that are commonly used to describe the structural changes induced by ligand binding. In the conformational selection model (Monod et al., 1965), the protein dynamically interchanges between multiple conformations and the ligand selectively binds and stabilises one conformation. In contrast, the induced-fit model (Koshland JR., 1959) describes the protein to initially exist in a conformation that is not fully complementary to the ligand and it undergoes a ligand-induced conformational change upon binding.

To characterise the structural changes of GAT1 upon sodium binding to NA1 and NA2 (Figure 4a), we first calculated the centre of mass (CoM) of the ion binding site(s), and then measured the average distance between the CoM and all coordinating oxygen atoms (Figure 4b,c) to quantify their compactness. The averaged compactness of NA1 and NA2 was determined in all simulations, which showed sodium binding, whereby each simulation was divided into the pre-binding and post-binding part (Figure 4 d,e). The mean compactness of NA1 remained unaffected by sodium binding (Figure 4d), while the breadth of the distribution increased slightly, indicating that in GAT1, sodium binding to the NA1 does not induce the same conformational change as observed for SERT (Szöllősi and Stockner, 2021). In contrast, the NA2 (Figure 4e) site showed after sodium binding a clear transition to a more compact geometry, reminiscent of an induced-fit mechanism.

The dynamics of Na1 and Na2 differed (Figure 4g). While Na2 was firmly bound to NA2, Na1 remained dynamic. Some trajectories showed an unbinding as Na1 returned to the temporary side and in a few trajectories subsequently bound to NA2. The low binding stability of Na1 is consistent with the lack of an induced fit effect and indicates that interactions of Na1 with the NA1 are weak. We use time Independent Component Analysis (tICA) (Molgedey and Schuster, 1994; Naritomi and Fuchigami, 2013), which is a dimension reduction method based on the slowest motions, in combination with Markov State Modelling (Zwanzig, 1983) that allows for quantifying the transition probabilities between microstates to derive the underlying free surface as implemented in PyEMMA (Scherer et al., 2015)sc. By applying this method, the simulation frames are first assigned the microstate in the to discretise functionally important conformational space as defined by the dimension reduction method tICA. In a second step, a Markov State Model is derived from the transition probabilities between the microstates as observed in the simulations. This analysis allows to derived the free energy landscape of sodium translational motions and to project them into the subspace of the slowest two motions as defined by tICA. The results showed a deep energy minimum for NA2 and a shallow minimum for NA1 (Figure 4h). Consistent with the repeatedly observed unbinding of Na1 and the transient binding of sodium to the temporary site before reaching NA1 or NA2, this temporary site in the S1 shows a broad and shallow energy minimum. The energy barrier separating NA1 for the temporary site is small, while a larger energy barrier separates the NA2 from the temporary site, supporting the interpretation of weak binding of Na1 and strong binding of Na2.

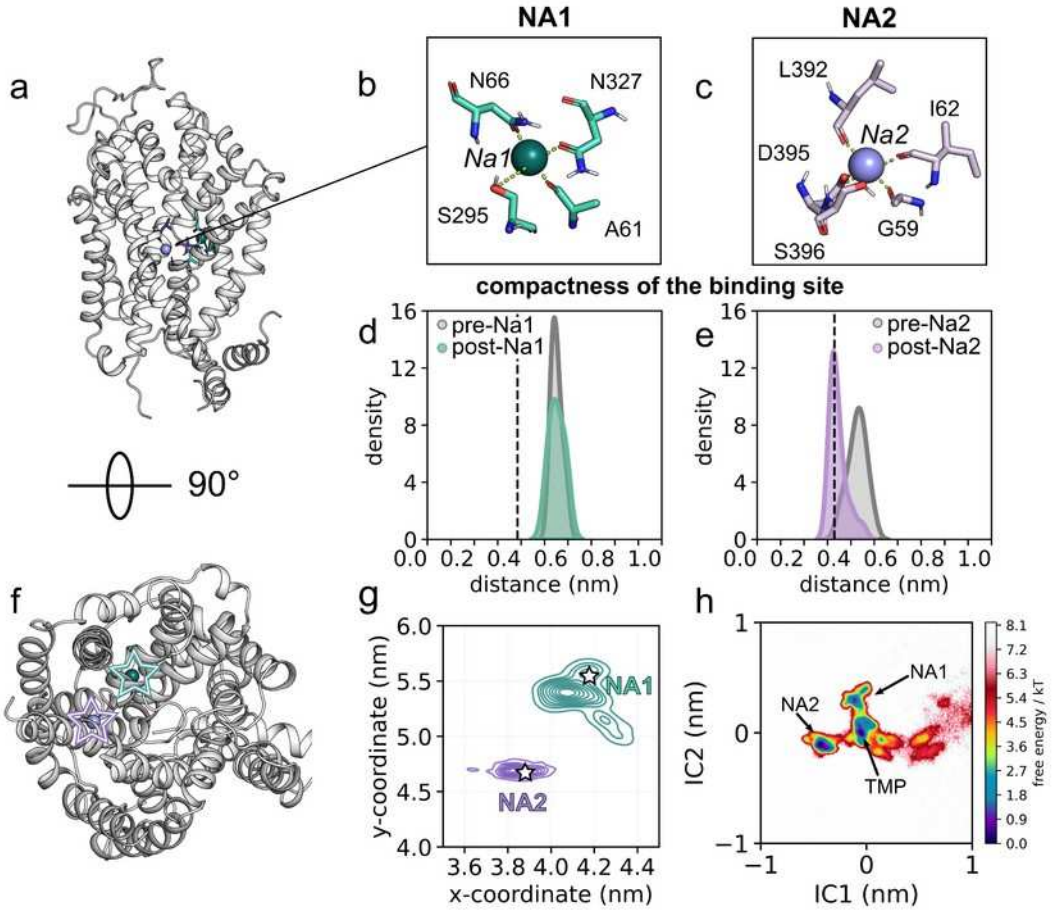

Figure 4. Short-range effect of sodium binding: ***a)*** *GAT1 structure represented as a cartoon, highlighting the ion binding sites* ***b)*** *Visualisation of the sodium binding sites NA1 (green) and* ***c)*** *NA2 (purple). The dashed lines indicate the distances used for determining the compactness NA1 and NA2.* ***d)*** *Compactness of NA1 and* ***e)*** *NA2 before (in grey) and after sodium binding (coloured according to panels a and b) The vertical dashed lines indicate the measure in the cryo-EM structure (PDB ID: 7Y7W), where GAT is pictured in a holo inward-occluded conformation.* ***f)*** *Reference orientation of GAT1 as used for panel g.* ***g)*** *Top view projection of sodium ion positional density after binding to NA1 and NA2. The canonical binding positions of Na1 and Na2 are indicated by stars.* ***h)*** *Free energy landscape of sodium binding, where coordinates are projected along IC1 and IC2, respectively.*

Na2 binding to the outward-facing conformation reduces internal transporter dynamics, thereby stabilising the closed inner gate and increasing structural integrity of TM5a

Next, we posed the question, if sodium binding to NA1 or NA2 would exert an allosteric effect on the overall transporter conformation and dynamics. We used principal component analysis (PCA) to identify the primary motions that occurred prior to and after sodium binding. PCA is a dimension reduction method that allows for identifying and extracting the motions with the largest amplitude in multidimensional data sets. We used PCA to project the dynamics of GAT1 onto the first two largest principal components (PCs) which represent the two motions with the largest amplitudes. Consistent with the lack of a compacting effect, we find that sodium binding to the NA1 did not have a global structural or dynamic effect of GAT1 (Figure S2). In contrast, binding of sodium to NA2 stabilised GAT1 in the outward-open conformation, which locally glued together TM1a and TM8. The projection of the two largest motions (PC1 and PC2) of GAT1 before and after sodium binding to NA2 (Figure 5 a,b) showed that GAT1 samples multiple conformations in the absence of Na2, consistent with a dynamic transporter. Upon sodium binding, the trajectories showed convergence towards the outward-open conformation, confirming that Na2 stabilises GAT1 in the outward-open state. Projection of motions along PC1 as β-factors on the TM helices of GAT1 (Figure 5c) showed that PC1 is mainly associated with motions of TM6a and that these large amplitude motions disappeared after binding of Na2 (Figure 5d), but also reduced mobility within TM5 (residue 242 to 245).

This data indicates that stabilisation of GAT1 in a specific conformation by Na2 is most likely a consequence of a reduction in bundle domain motions (Figure 5 e,f). Similar to PCA, maximum likelihood structural alignment and correlation analysis showed that the largest motion of GAT1 prior to Na2 binding were concerted motions of the bundle domain relative to the scaffold domain. The motions of bundle and scaffold domains at the outer and the inner vestibule were anticorrelated with respect to each other, which is consistent with the rocking bundle model of SLC6 transporter motions. Consistent with the PCA analysis, at the cytosolic side the first part of TM5a showed large motions. Upon binding of Na2, the transporter dynamics were very different. Motions of the bundle domain relative to the scaffold domain were strongly diminished and breathing motions between the extracellular ends of TM5 and TM11 dominated. Na2 binding has therefore a long range effect on the entire bundle domain, but also on TM5a, which contributes to the formation of the inner hydrophobic gate.

Na2 makes an important contribution to the stabilisation of the inner gate. To quantify the dynamics of the inner gate, we measured two orthogonal distances at the hydrophobic inner gate (Figure 5h): the contact across the hydrophobic inner gate between F51 (TM1a) and Y241 (TM6), as well as a measure of the length of TM5a by determining the distances between Y227 (TM4) as fixed reference point and Y248 on TM5a. Figure 5g shows distance distribution plots for the two measures. We found that the inner hydrophobic gate is dynamic in the absence of Na2, as GAT1 oscillates by 1 nm along the axis of inner gate opening (F51-Y241), indicating structural instability. The gate stabilised in the closed conformation in the presence of Na2, leading to a single main distance at ~0.8 nm. Similar to the stability of the inner hydrophobic gate, TM5a (Figure 5g) showed a broader distribution in the absence of Na2. It condensed to a single main distance of ~1.9 nm after Na2 binding, indicating that Na2 has a long range effect on TM5a that leads to its stabilisation. Consistent with GAT1, movements of TM5a have been associated with opening of the inner gate at other members of the SLC6 transporter family (Coleman et al., 2019; Merkle et al., 2018).

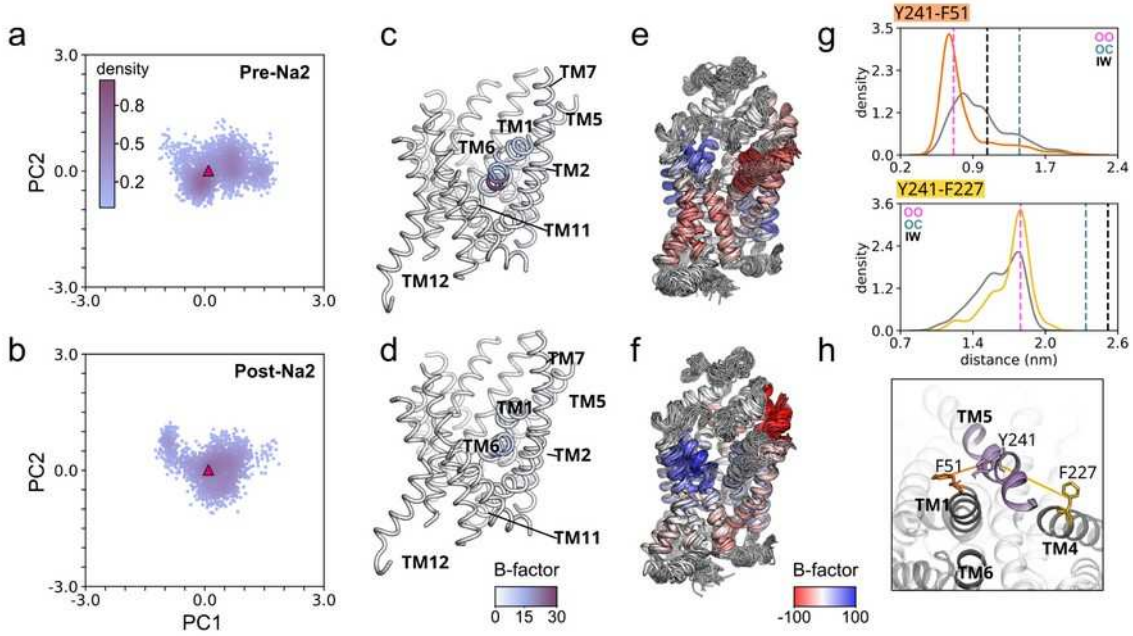

Figure 5. Global structural effects of sodium binding to NA2: *Scatter plot of principal component 1 (PC1) against PC2 of all simulations that showed NA2 binding. Trajectories are divided into* ***a)*** *before and* ***b)*** *after Na2 binding. The pink triangle corresponds to the outward-open AlphaFold model of GAT1. All trajectories are projected to the same PC1 and PC2 axis. (****c,d****) Root Mean Square Fluctuations (RMSF) of motions along PC1 mapped as β-factors on the TM helices of GAT1 for the frames* ***c)*** *before Na2 binding and* ***d)*** *after Na2 binding. (****e, f****) Using the same orientation as in panel c, superpositioning of 1 ns separated frames with the maximum likelihood method. Structures are coloured according to the degree of correlated motions along PC1 for frames* ***e)*** *before Na2 binding and* ***f)*** *after Na2 binding.* ***g)*** *Density distribution of the distances Y241-F51 and Y241-F227 visualised in panel h, where values before Na2 binding are shown in grey, and after Na2 binding are coloured according to the legend. The vertical dashed lines indicate the distance measured in the cryo-EM structures of the GAT1 holo occluded and apo inward-open conformations (PDB ID: 7Y7W, 7Y7V) (Zhu et al., 2023) and in the AlphaFold outward-open model* ***h****) The distances shown in panels g are indicated in orange between TM1a (F51) and TM5a (Y241), and in yellow between TM4 (F227) and TM5b (Y241).*

Role of NA1 in substrate binding

The behaviour of Na1 differs between the paralogue transporters SERT and GAT1. In SERT, Na1 binds tightly and the NA1 changes conformation according to an induced fit effect (Szöllősi and Stockner, 2021). A key difference between SERT and GAT1 is the Na1 coordinating carboxylate moiety (Figure 6b). In SERT, the carboxylate moiety is donated by the conserved aspartate residue D98, while in GAT1, the corresponding residue is a conserved glycine (G63) and, similar to LeuT (Yamashita et al., 2005), the carboxylate moiety of the substrate completes the Na1 (Figure 6c) coordination shell in GAT1.

To test this hypothesis, we docked GABA into sodium and chloride bound GAT1, carried out four independent 0.5 µs long simulations and compared the trajectories to four 0.5 µs long simulations in the absence of GABA (Figure 6d-g). Consistent with the sodium binding

simulations, Na1 was unstable and temporarily unbound from the NA1 in the absence of GABA, moving to the temporary site, but remaining within the S1. The compactness of the NA1 (Figure 6e) was consistent with the compactness of the NA1 as observed in the sodium binding simulations (Figure 4c). Simulations carried out in the presence of GABA were strikingly different: Na1 remained stably bound and the NA1 and the NA1 was more compact. The compacting of the NA1 was reminiscent of an induced fit effect (Figure 6g). This data shows that the carboxylate moiety is essential for completing NA1 and is required to stabilise the Na1.

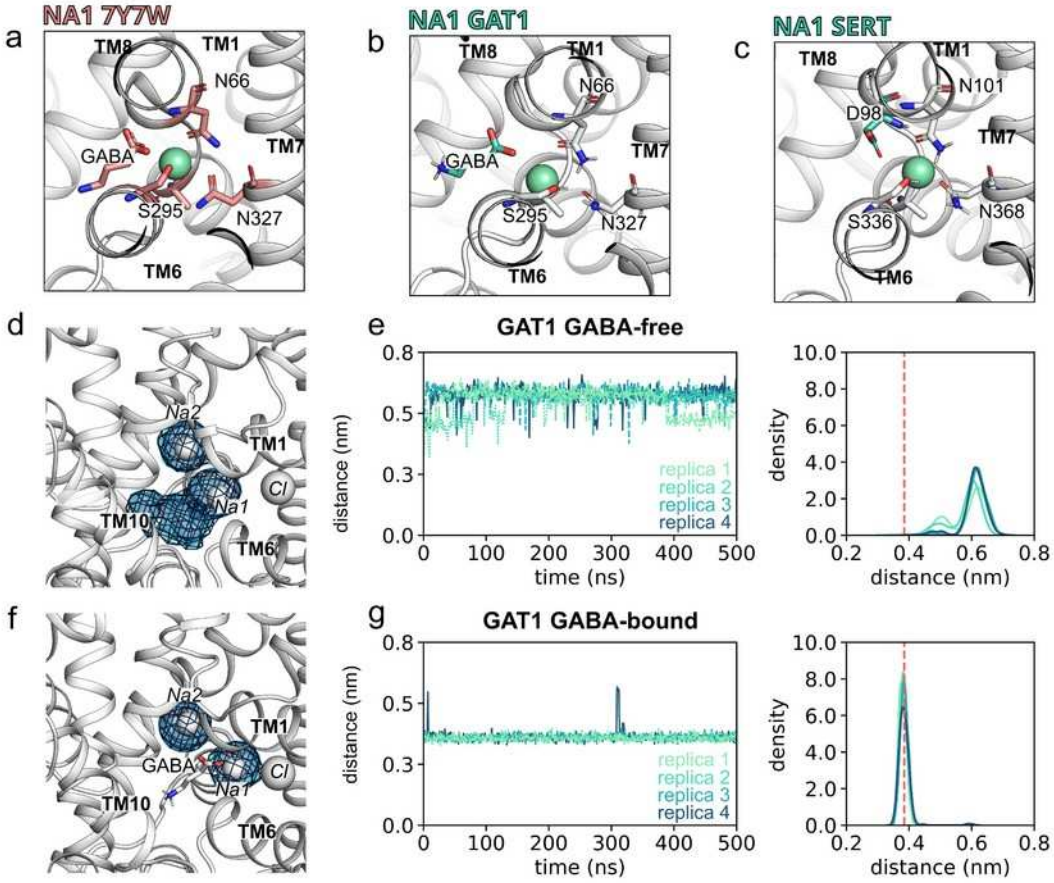

Figure 6. The substrate GABA completes the sodium binding site NA1: a-c) Comparison of the sodium binding site NA1 in **a)** the cryo-EM holo inward-occluded GAT1 (PDB ID: 7y7w (Zhu et al., 2023), **b)** AlphaFold holo outward-open GAT1, **c)** and SERT. The group donating the sodium-coordinating carboxylate moiety is GABA in GAT1 (a, b) and D98 in SERT c). **d)** Zoom onto S1 showing as isomesh surfaces the regions in which sodium ions Na1 and Na2 are found in the four 0.5 μs long simulations in the absence of GABA. **e**) Time course and averaged histogram of the compactness of NA1. The vertical dashed line highlights the measured NA1 compactness in the holo inward-occluded GAT1 cryo-EM structure (PDB ID: 7Y7W (Zhu et al., 2023) **f,g)** Same as in panels d, and e, but in the presence of GABA.

Discussion

The importance of sodium for substrate transport has been characterised at the macroscopic and the kinetic level (Hilgemann and Lu, 1999; Iversen and Snyder, 1968; Mager et al., 1993) and showed that GABA uptake is energised by the downhill concentration gradient of the co-transported sodium (Kanner, 1978). Structural data of transporters from the SLC6 family have revealed the binding sites of substrate and co-transport ions and the main conformations of the transport cycle of GAT1 (Nayak et al., 2023; Zhu et al., 2023).

We confirmed through direct observations that NA2 functions to stabilise GAT1 in the outward-open conformation and showed that Na2 achieves this by immobilising the scaffold and bundle domains in relation to each other. Meanwhile, NA1 plays a crucial role in securing the GAT1 substrate by directly interacting with its carboxylate component, forming the essential connections that constitute the primary coordination environment of Na1.

Despite all this information, it is not completely clear how the sodium ions would be able to control the GABA transporter at the molecular level. The free energy landscape showed that NA2 binds sodium much stronger than NA1, and that the energy barrier connecting NA1 with a temporary site in the S1 is small. This is reflected in the dynamics of sodium ions. Simulations showed a clear order for sodium binding: the first stably bound sodium entered the NA2 and stabilised the outward-open conformation, thereby priming GAT1 for substrate binding. Once bound to the NA2, we did not observe any indication for unbinding of Na2 during the time course of the simulation. Sodium ions which initially interacted with NA1 remain mobile, eventually returning to the temporary site in the S1 and eventually binding to the NA2 (if empty). The second sodium ion that is electrostatically attracted to the S1 remains in a loose binding state as it keeps oscillating between the NA1 and the temporary site, because the NA1 remains incomplete until a substrate reaches the S1.

The role of Na2 is to stabilise GAT1 in the outward-open conformation. It was shown for LeuT that the transporter isomerizes between the inward-facing and the outward-facing state with comparable populations for both conformations in the absence of sodium ions, while the presence of sodium stabilises the outward-facing conformation (Zhao et al., 2011). A similar conformational effect upon sodium binding was observed for human SLC6 transporters (Schicker et al., 2012; Tavoulari et al., 2016; Zhang et al., 2018), because the NA2 is located between the scaffold domain and the bundle domain, specifically between TM1a and TM8 (Krishnamurthy and Gouaux, 2012; Yamashita et al., 2005). NA2 becomes disrupted by a transition to the inward-facing state. These data remained inconclusive with respect to the functionally important question, if Na2 would stabilise the NA2 and thus the transporter in the outward-open state or if the outward-open state would be formed by other interactions and thereby creating the sodium binding competent NA2. Our data showed that it is Na2 binding that stabilises GAT1. We observed that GAT1 is dynamic in the outward-open state and showed large bundle domain motions on both the extracellular and also the intracellular side in the absence of Na2. This is consistent with a dynamic state reminiscent of the apo state of LeuT without conformational preference (Zhao et al., 2011). We also observed motions at the inner gate, specifically between TM5a and the bundle domain helices TM1a and TM6b, which indicates that Na2 binding plays a long range stabilising role for the inner gate and for TM5a. A closed hydrophobic inner gate is necessary for stabilising the outward-facing state, while it has to open for reaching the inward-open state. We found a dynamic inner gate in the absence of Na2, as we measured broad distributions of distances across the inner gate. A long range effect of Na2 binding resulted in the disappearance of these dynamic motions, leading to the stabilisation of a sealed inner gate. We find that a long range allosteric effect of Na2 binding is a stabilisation of the conformation of TM5a, reminiscent of the observations in the homologous transporters LeuT and SERT (Coleman et al., 2019; Merkle et al., 2018),

which showed an unwinding and an extension of TM5a in the transition from the outward-facing to the inward-facing state.

The motions of the bundle domain, responsible for this property, were quenched after sodium binding to NA2, showing how Na2 stabilises the outward-open state. The conformation stabilising effect of Na2 is achieved by an induced fit effect. Analysis of the local environment of the sodium coordinating oxygen atoms at the NA2 showed a clear structural change upon sodium binding that brought the NA2 exposed residues of TM1a and TM8 into a defined distance that is smaller than these residues would be in the absence of Na2. This local structural change fixes these two helices relative to each other and thereby prevents bundle domain motions relative to the scaffold domain, as TM1a is part of the bundle domain and TM8 is part of the scaffold domain.

The NA1 site has the role of stabilising the bound substrate in the S1. The apparent affinity of GABA for GAT1 increases strongly in the presence of sodium (Radian and Kanner, 1983). Here we show that binding of Na1 and of GABA is synergistic, as GABA stabilises Na1 in the NA1 and Na1 stabilises GABA in the S1. We observed by direct simulations that sodium oscillated between the NA1 and a temporary site in the S1 without induced fit conformational changes of NA1 in the absence of substrate. In contrast, in the presence of GABA, sodium is firmly bound to the NA1, the carboxylate moiety of GABA completes the first coordination shell of Na1 and NA1 compacts. The same position for the carboxylate was found in the occluded structure of GAT1 (Zhu et al., 2023). As yet no structural information on Na bound GAT1 in the absence of GABA is available, but different coordinations of Na1 in LeuT were observed in the absence and presence of the coordinating carboxyl group of the amino acid substrate (Krishnamurthy and Gouaux, 2012), it is likely that this difference in Na1 coordination is similar in GAT1. The carboxyl group of GABA overlaps with the carboxylate of D98 in the paralogues serotonin transporter SERT, where sodium binds strongly in the absence of substrate and the NA1 compacts due to an induced fit effect (Szöllősi and Stockner, 2021). The difference between GAT1 and SERT is therefore that strong binding of Na1 and NA1 condensation in GAT1 is GABA dependent, while in the SERT it is substrate independent. From this data we can infer that the strong electrostatic interactions between the negatively charged carboxylate of GABA and the positive charge of sodium as well as the condensation of NA1 due to the induced fit effect contribute cooperatively to the affinity of GABA to GAT1. GABA adopts a binding mode in which the carboxyl group completes the coordination of sodium of NA1, but is also stabilised by a hydrogen bond to Y140 of the scaffold domain. It is tempting to speculate that this interaction relay from Na1 (bundle domain associated), GABA to Y140 (scaffold domain) could be the switch that triggers GAT1 occlusion and thus substrate uptake reminiscent of the mechanism described by Gradish et al. (Gradisch et al., 2022)

Binding of sodium and substrate transport by GAT1 is accelerated by a sodium recruitment site. Our simulations showed consistently a region of high sodium density at the entry to the outer vestibule. The sodium recruiting site consists of two negatively charged residues located at the beginning of TM6a that electrostatically attracts sodium ions. *In-silico* mutations of these residues resulted in the disappearance of enhanced sodium density at the sodium recruiting site and slowed binding kinetics (slower on rate) for sodium entering into the S1 (Figure 1). *In-vitro* experiments confirmed these predictions (Figure 3) by showing a reduced sodium dependency of GABA uptake and a lower V_{max}, while the K_M of GABA uptake was almost unchanged. These data indicate that the role of the sodium recruiting site is to increase the probability of sodium ions to enter the outer vestibule for reaching the sodium binding sites NA1 and NA2. The negative electrostatic potential at the

sodium recruiting site attracts positively charged sodium ions and locally increased sodium concentration at the entry into the outer vestibule. We did not observe tight binding to the recruitment site, but instead observed that sodium ions eventually unbind. This is kinetically important, because increasing the on rate, as the sodium ion can leave either towards the extracellular solution or it is efficiently steered towards the S1 by electrostatic attraction.

Material and Methods

Molecular Dynamics simulations

In the absence of a crystal or cryo-EM structure of GAT1 in the outward-facing conformation, we selected the AlphaFold *homology* model to investigate sodium binding (Jumper et al., 2021; Varadi et al., 2022).

The bound-chloride ion was added to the GAT1 model using as a reference of the outward-open human SERT crystal structure (PDB ID: 5I71; (Coleman et al., 2016). The generated system was converted from full-atom into a coarse-grained representation using the MARTINI force field (de Jong et al., 2013; Monticelli et al., 2008; Wassenaar et al., 2015), with a membrane composition of 1-palmitoyl-2-oleoyl phosphatidylcholine (POPC): cholesterol containing membrane (POPC:CHOL 70:30 mol%; (van Meer, 1998), and solvated in water with 150 mM NaCl. After a 1 μs long coarse-grained simulation, while restraining the protein structure, the membrane was equilibrated. The coarse-grained system was then converted to an all-atom representation (Ingólfsson et al., 2014) in which the transporter was replaced by the original GAT1 model to avoid spurious structural imprecisions induced by the double coordinate conversion protocol. Possible atom overlaps between the reinserted protein and the equilibrated membrane were relaxed using the membed procedure (Wolf et al., 2010) as previously described (Szöllősi and Stockner, 2022). We used the amber ff99SB-ILDN force field (Lindorff-Larsen et al., 2010) to describe GAT1, ions and the solvent, and Slipid (Jämbeck et al., 2013; Jämbeck and Lyubartsev, 2013) for POPC and cholesterol. Previously reported structural analysis of the orthologous SERT structure (Coleman et al., 2016) suggested that the residue E467 in GAT1 is protonated. All simulations were carried out with GROMACS version 2019.2 (Abraham et al., 2015). Three replicas of the final assembled system were energy-minimised and equilibrated in four steps of 2.5 ns, each by stepwise releasing the position restraints (1,000, 100, 10, 1 kJ/mol/nm) that are active on the Cα atoms and the bound chloride ion (Goda et al., 2020; Sohail et al., 2016). Per each trajectory, the production run was carried for 500 ns. The temperature was maintained at 310 K using the v-rescale (τ = 0.5 ps) thermostat (Bussi et al., 2007), while separately coupling protein, membrane, and solvent. The pressure was maintained at 1 bar using the Parrinello-Rahman barostat (Parrinello and Rahman, 1981) in a semi-isotropic manner and applying a coupling constant of 20.1 ps. Long-range electrostatic interactions were described using the smooth particle mesh Ewald method (Darden et al., 1993) applying a cutoff of 0.9 nm. The van der Waals interactions were described using the Lennard Jones potentials applying a cutoff of 0.9 nm. Long-range corrections for energy and pressure were applied. Coordinates of all atoms were recorded every 5 ps. The complete set of parameters of the production run can be found in the Supplementary Materials.

The resulting trajectories were used as parent trajectories to extract starting structures for the sodium binding simulations. From each replica, 20 equally spaced frames were extracted

every 10 ns of the 200 ns long trajectories, which then served as starting structures after removal of sodium ions that might be present in the substrate binding pocket S1. Each of these 60 systems was simulated for 200 ns with the same simulation parameters as the parent trajectories. The same starting systems were used for the double mutant (D281A-E283A) systems and the same simulation parameters were applied. Mutants were created using the Pymol Mutagenesis Wizard tool (Schrödinger, LLC, Warren DeLano, 2020).
To generate the trajectory for investigating the role of sodium Na1, we extracted a frame from the parent trajectory in which Na2 was already bound. For the GABA-free systems, we placed the second sodium into the temporary site of the S1 as observed in the sodium binding simulations; for the GABA-bound systems we placed GABA in the binding site of GAT1, in a similar way as leucine was observed in the LeuT crystal structure (Yamashita et al., 2005). Figures and statistical analyses were generated by the GROMACS package, R, and python scripts using the MD Analysis package, v0.19.2 (Gowers et al., 2016; Michaud-Agrawal et al., 2011). For visualisation VMD (Humphrey et al., 1996) v1.9.3 and Pymol v1.8.4 (Schrödinger, LLC, Warren DeLano, 2020) were used.

Markov State Modelling

The Markov State Models (MSMs) were built with pyEMMA python package version 2.5.9 (Scherer et al., 2015). To begin, we defined the reaction coordinates employing time-lagged Independent Component Analysis (tICA) (Molgedey and Schuster, 1994; Naritomi and Fuchigami, 2013), an advanced linear transformation technique design to maximise the autocorrelation of molecular descriptors. This facilitates the identification of slowest kinetic modes within the system, i.e., the reaction coordinates. The input dataset for tICA comprised the precise coordinates (x, y and z) of the sodium ions undergoing binding events. The dimensional reduction was performed using time lag of 1 ns which allowed for a complete exploration of the temporal dynamics. Subsequently, the trajectories were discretized into 500 cluster centres by applying the k-mean clustering algorithm. Finally, the MSMs were estimated using a time lag of 25 ns, the time point we observed convergence of the implied timescales. Additionally, the markovian behaviour was assured using Chapman-Kolmogorov (CK) test [SI figure].

The free energy values were estimated using the MSMs based on the relationship derived from the stationary distribution (π) values, as obtained from the transition probability matrix [citation needed]. This relationship is represented mathematically as GSj=-KbTln (sum(πj)). Where j denotes the MSM stationary weight of the jth microstate. G, S, Kb and T represent the Gibbs free energy, entropy, Boltzmann constant and temperature, respectively. To visualise and interpret the free energy landscape associated with sodium binding, we plotted the free energy values into the tICA subspace, specifically along the first and second slowest motions, IC1 and IC2.

Cell lines and cell culture

An N-terminal eYFP tagged human GAT1 wildt-ype plasmid was used, QuickChange primers as well as the QuickChange II site-directed mutagenesis kit (Agilent Technologies,

Santa Clara, USA) were used to incorporate point mutations into human GAT1. After construct verification (LGC Genomics, Berlin, Germany) double sorted polyclonal HEK293 cell lines, stably and consistently expressing hGAT1 wild-type as well as the double alanine variant (D281A-E283A) were established. Therefore, raw HEK cells were transfected with the respective plasmid by applying the jetPRIME transfection protocol (VWR International GmBH, Vienna, Austria). Adding 100 µl geneticin (G418, 50 mg x ml^{-1}) ensured high selection pressure which was maintained for at least 14 days before cells were FACS sorted. Subsequently cells were grown for 1 week followed by a second round of FACS sorting.

Cells stably expressing GAT1 were grown in 10 cm cell culture dishes (Greiner) with Dubleco's Modified Eagle Media (DMEM, Sigma-Aldrich, St. Louis, USA) supplemented with 10% heat-inactivated Fetal Bovine Serum (FBS, Sigma Aldrich), penicillin (1 U x ml^{-1}, Sigma Aldrich), streptomycin (100 µg x ml^{-1}, Sigma Aldrich) and geneticin (50 µg x ml^{-1}, Sigma Aldrich) at 37 °C and 5 % CO2 in an incubator. Regular tests for mycoplasma were performed by 4′,6-diamidino-2-phenylindole staining.

Confocal microscopy

A day prior to live confocal imaging the cells were seeded onto poly-D-lysine (PDL)-coated 35 mm glass-bottom dishes (Cellvis, Sunnyvale, California, USA) at a density of 0.2 x 10^6 cells per 2 ml). After aspiration of the culture medium, cell membranes were stained with a 0.4% Trypan blue containing solution (Sigma) for 10 minutes. Subsequently, cells were washed several times with Krebs-HEPES buffer (KHP, 10 mM HEPES, 120 mM NaCl, 3 mM KCl, 2 mM CaCl2, 2 mM MgCl2, 2 mM glucose monohydrate, pH 7.3) and kept on KHB throughout the imaging process. Cell imaging was performed using a Nikon A1R+ laser scanning confocal microscope equipped with a 60x NA1.4 oil immersion objective (Nikon, Vienna, Austria). To visualise Trypan blue and eYFP fluorescence, laser lines at 561 nm and 488 nm were employed, respectively. Prior light detection by a GaAsP PMT detector, emitted light was filtered with a 595/50 nm (trypan blue) and 525/50 (eYFP) nm emission filter. Image analysis was performed by using Fiji ImageJ 1.53c. Trypan blue staining confined both regions of interest (ROI) used to measure surface expression as well as cytosolic retained transporters. Both measurements were defined by mean fluorescence over the confined ROI.

Radiotracer Uptake assays

Cells were seeded (~0.05 x 10^6 cells / 0.2 ml / well) onto PDL-coated 96-well plates a day before the experiment. After removal of the culture medium cells were kept on KHP throughout the experiment. Concentration-dependent uptake was determined by applying solutions containing 50 nM [^{3}H]GABA and increasing concentrations of GABA (0.15 - 59.95 µM) for 3 minutes at room temperature. Thereafter, cells were washed with 500 µl ice-cold KHB to terminate the uptake and subsequently lysed by adding 200 µl Ultima Gold Scintillation Cocktail (Sigma).

In case of determining the sodium-dependence of GAT1-mediated [^{3}H]GABA uptake, cells were kept in KHP with varying concentrations of sodium (0 mM - 200 mM). To compensate for changes in osmolarity N-methyl D-glucamine (NMDG)-chloride was added accordingly (200 mM - 0 mM). Uptake solutions (KHB with varying concentrations of sodium and NDMG-Cl) containing 50 nM [^{3}H]GABA were added to the cells for 3 minutes, followed by aspiration and a washing step with 500 µl ice-cold KHB. Cell lysis was achieved by adding 200 µl of Ultima Gold Scintillation Cocktail. Non-specific uptake was determined in presence of 10 µM

tiagabine. A ß-scintillation counter (Perkin Elmer, Waltham, USA) was used to quantify the uptake of [^{3}H]GABA.

Whole-cell patch clamp

24 hours prior the experiment cells were seeded at very low density onto PDL-coated 35 mm dishes. hGAT1-mediated and substrate induced currents were recorded in whole-cell configuration at a holding-potential of -60 mV. Throughout the experiments cells were maintained in regular external solution (bath solution) containing: 140 mM NaCl, 20 mM D-glucose, 10 mM HEPES, 3 mM KCl, 2.5 mM $CaCl_2$, 2 mM $MgCl_2$, pH adjusted to 7.4 with NaOH. The patch pipette harbours regular internal solution comprises: 133 mM K^+-gluconate, 10 mM HEPES, 10 mM EGTA, 5.9 mM NaCl, 1 m $CaCl_2$, 0.7 mM $MgCl_2$, pH adjusted to 7.2 with KOH. An 8 tube ALA perfusion manifold (NPI Electronic GmbH, Germany) and a DAD-12 superfusion system (Adams & List, Westbury, NY) ensured fast drug perfusion onto the cell and complete solution exchange surrounding the cell within ~ 100ms. GABA was applied for 5 seconds. After passive holding currents were subtracted, the traces were filtered by applying a 100 Hz digital Gaussian low-pass filter as well as a 50 Hz harmonics filter. Clampfit 10.2 was used to analyse the current amplitudes. Data analysis was performed by using GraphPad Prism version 9.4.1. At least 6 independent cells have been recorded.

Data and statistical analysis

Experimentally acquired data were analysed and plotted with GraphPad Prism 9.5.1 (GraphPad Software Inc., San Diego, USA). Michaelis Menten kinetics (K_m, V_{max}) were determined solving the following equation: $Y = Vmax*X/(Km + X)$. EC_{50} values deduced from electrophysiological recordings were determined as follows: Y=Bottom + (Top-Bottom)/(1+10^((LogEC50-X))). The affinity for sodium (EC_{50}) was calculated by solving: Y=Bottom + (X^Hillslope)*(Top-Bottom)/(X^HillSlope + EC50^HillSlope). All data are from at least five biologically independent experiments ($n \geqslant 5$), measured in triplicates and reported as mean ± SD. In case of electrophysiological measurements a minimum of 8 individual cells were recorded and plotted as mean ± SD. *Statistics were conducted by applying the paired t-test. *=P < 0.0332, **=P < 0.0021, ***P < 0.0002, ****P < 0.0001.*

Funding Information

This work has received funding from the European Union H2020-MSCA-ITN 2019, grant agreement No 860954. Additionally, financial support from the Austrian Science Foundation (FWF), grant No. P34670-B to HHS, P32017 to TS and P36574 to SS gratefully acknowledged.

Author Contributions

Erika Lazzarin, Conceptualization, Data curation, Formal analysis, Investigation, Methodology, Writing – Original Draft Preparation; Ralph Gradish, Conceptualization, Data curation, Formal analysis, Investigation, Review & Editing; Sophie M.C. Skopec, Investigation, Formal analysis, Methodology; Leticia Alves da Silva, Investigation, Methodology, Software; Dániel Szöllősi, Methodology, Software, Writing – Review & Editing; Harald H Sitte, Resources, Supervision, Funding acquisition, Writing – Review & Editing; Julian Maier, Investigation, Writing – Review & Editing; Sonja Sucic, Funding acquisition, Resources, Writing – Review & Editing; Baruch I. Kanner, Writing – Review & Editing; Thomas Stockner, Writing – Conceptualization, Project Administration, Resources, Supervision ,Writing – Original Draft Preparation, Writing – Review & Editing

References

Abraham, M.J., Murtola, T., Schulz, R., Páll, S., Smith, J.C., Hess, B., Lindahl, E., 2015. GROMACS: High performance molecular simulations through multi-level parallelism from laptops to supercomputers. SoftwareX 1–2, 19–25. https://doi.org/10.1016/j.softx.2015.06.001

Bhat, S., El-Kasaby, A., Freissmuth, M., Sucic, S., 2021. Functional and Biochemical Consequences of Disease Variants in Neurotransmitter Transporters: A Special Emphasis on Folding and Trafficking Deficits. Pharmacol. Ther. 222, 107785. https://doi.org/10.1016/j.pharmthera.2020.107785

Bhatt, M., Gauthier-Manuel, L., Lazzarin, E., Zerlotti, R., Ziegler, C., Bazzone, A., Stockner, T., Bossi, E., 2023. A comparative review on the well-studied GAT1 and the understudied BGT-1 in the brain. Front. Physiol. 14.

Bicho, A., Grewer, C., 2005. Rapid substrate-induced charge movements of the GABA transporter GAT1. Biophys. J. 89, 211–231. https://doi.org/10.1529/biophysj.105.061002

Bussi, G., Donadio, D., Parrinello, M., 2007. Canonical sampling through velocity rescaling. J. Chem. Phys. 126, 014101. https://doi.org/10.1063/1.2408420

Chen, N.-H., Reith, M.E.A., Quick, M.W., 2004. Synaptic uptake and beyond: the sodium- and chloride-dependent neurotransmitter transporter family SLC6. Pflugers Arch. 447, 519–531. https://doi.org/10.1007/s00424-003-1064-5

Coleman, J.A., Green, E.M., Gouaux, E., 2016. X-ray structures and mechanism of the human serotonin transporter. Nature 532, 334–339. https://doi.org/10.1038/nature17629

Coleman, J.A., Yang, D., Zhao, Z., Wen, P.-C., Yoshioka, C., Tajkhorshid, E., Gouaux, E., 2019. Serotonin transporter–ibogaine complexes illuminate mechanisms of inhibition and transport. Nature 569, 141–145. https://doi.org/10.1038/s41586-019-1135-1

Darden, T., York, D., Pedersen, L., 1993. Particle mesh Ewald: An N·log(N) method for Ewald sums in large systems. J. Chem. Phys. 98, 10089–10092. https://doi.org/10.1063/1.464397

de Jong, D.H., Singh, G., Bennett, W.F.D., Arnarez, C., Wassenaar, T.A., Schäfer, L.V., Periole, X., Tieleman, D.P., Marrink, S.J., 2013. Improved Parameters for the Martini Coarse-Grained Protein Force Field. J. Chem. Theory Comput. 9, 687–697. https://doi.org/10.1021/ct300646g

Fischer, F.P., Kasture, A.S., Hummel, T., Sucic, S., 2022. Molecular and Clinical Repercussions of GABA Transporter 1 Variants Gone Amiss: Links to Epilepsy and Developmental Spectrum Disorders. Front. Mol. Biosci. 9.

Forrest, L.R., Zhang, Y.-W., Jacobs, M.T., Gesmonde, J., Xie, L., Honig, B.H., Rudnick, G., 2008. Mechanism for alternating access in neurotransmitter transporters. Proc. Natl. Acad. Sci. 105, 10338–10343. https://doi.org/10.1073/pnas.0804659105

Ghit, A., Assal, D., Al-Shami, A.S., Hussein, D.E.E., 2021. GABAA receptors: structure, function, pharmacology, and related disorders. J. Genet. Eng. Biotechnol. 19, 123. https://doi.org/10.1186/s43141-021-00224-0

Goda, K., Dönmez-Cakil, Y., Tarapcsák, S., Szalóki, G., Szöllősi, D., Parveen, Z., Türk, D., Szakács, G., Chiba, P., Stockner, T., 2020. Human ABCB1 with an ABCB11-like degenerate nucleotide binding site maintains transport activity by avoiding nucleotide occlusion. PLOS Genet. 16, e1009016. https://doi.org/10.1371/journal.pgen.1009016

Gowers, R., Linke, M., Barnoud, J., Reddy, T., Melo, M., Seyler, S., Domański, J., Dotson,

D., Buchoux, S., Kenney, I., Beckstein, O., 2016. MDAnalysis: A Python Package for the Rapid Analysis of Molecular Dynamics Simulations. Presented at the Python in Science Conference, Austin, Texas, pp. 98–105. https://doi.org/10.25080/Majora-629e541a-00e

Gradisch, R., Szöllősi, D., Niello, M., Lazzarin, E., Sitte, H.H., Stockner, T., 2022. Occlusion of the human serotonin transporter is mediated by serotonin-induced conformational changes in the bundle domain. J. Biol. Chem. 298, 101613. https://doi.org/10.1016/j.jbc.2022.101613

Guastella, J., Nelson, N., Nelson, H., Czyzyk, L., Keynan, S., Miedel, M.C., Davidson, N., Lester, H.A., Kanner, B.I., 1990. Cloning and Expression of a Rat Brain GABA Transporter. Science 249, 1303–1306. https://doi.org/10.1126/science.1975955

Hasenhuetl, P.S., Freissmuth, M., Sandtner, W., 2016. Electrogenic Binding of Intracellular Cations Defines a Kinetic Decision Point in the Transport Cycle of the Human Serotonin Transporter. J. Biol. Chem. 291, 25864–25876. https://doi.org/10.1074/jbc.M116.753319

Hilgemann, D.W., Lu, C.-C., 1999. Gat1 (Gaba:Na+:Cl−) Cotransport Function: Database Reconstruction with an Alternating Access Model. J. Gen. Physiol. 114, 459–476. https://doi.org/10.1085/jgp.114.3.459

Humphrey, W., Dalke, A., Schulten, K., 1996. VMD: Visual molecular dynamics. J. Mol. Graph. 14, 33–38. https://doi.org/10.1016/0263-7855(96)00018-5

Ingólfsson, H.I., Melo, M.N., van Eerden, F.J., Arnarez, C., Lopez, C.A., Wassenaar, T.A., Periole, X., de Vries, A.H., Tieleman, D.P., Marrink, S.J., 2014. Lipid Organization of the Plasma Membrane. J. Am. Chem. Soc. 136, 14554–14559. https://doi.org/10.1021/ja507832e

Iversen, L.L., Snyder, S.H., 1968. Synaptosomes: Different Populations storing Catecholamines and Gamma-aminobutyric Acid in Homogenates of Rat Brain. Nature 220, 796–798. https://doi.org/10.1038/220796a0

Jämbeck, J.P.M., Lyubartsev, A.P., 2013. Another Piece of the Membrane Puzzle: Extending Slipids Further. J. Chem. Theory Comput. 9, 774–784. https://doi.org/10.1021/ct300777p

Jämbeck, J.P.M., Mocci, F., Lyubartsev, A.P., Laaksonen, A., 2013. Partial atomic charges and their impact on the free energy of solvation. J. Comput. Chem. 34, 187–197. https://doi.org/10.1002/jcc.23117

Jumper, J., Evans, R., Pritzel, A., Green, T., Figurnov, M., Ronneberger, O., Tunyasuvunakool, K., Bates, R., Žídek, A., Potapenko, A., Bridgland, A., Meyer, C., Kohl, S.A.A., Ballard, A.J., Cowie, A., Romera-Paredes, B., Nikolov, S., Jain, R., Adler, J., Back, T., Petersen, S., Reiman, D., Clancy, E., Zielinski, M., Steinegger, M., Pacholska, M., Berghammer, T., Bodenstein, S., Silver, D., Vinyals, O., Senior, A.W., Kavukcuoglu, K., Kohli, P., Hassabis, D., 2021. Highly accurate protein structure prediction with AlphaFold. Nature 596, 583–589. https://doi.org/10.1038/s41586-021-03819-2

Kanner, B.I., 1978. Active transport of γ-aminobutyric acid by membrane vesicles isolated from rat brain. Biochemistry 17, 1207–1211. https://doi.org/10.1021/bi00600a011

Kasture, A.S., Fischer, F.P., Kunert, L., Burger, M.L., Burgstaller, A.C., El-Kasaby, A., Hummel, T., Sucic, S., 2023. Drosophila melanogaster as a model for unraveling unique molecular features of epilepsy elicited by human GABA transporter 1 variants. Front. Neurosci. 16.

Keynan, S., Kanner, B.I., 1988. gamma-Aminobutyric acid transport in reconstituted

preparations from rat brain: coupled sodium and chloride fluxes. Biochemistry 27, 12–17. https://doi.org/10.1021/bi00401a003

Kortagere, S., Fontana, A.C.K., Rose, D.R., Mortensen, O.V., 2013. Identification of an allosteric modulator of the serotonin transporter with novel mechanism of action. Neuropharmacology 72, 282–290. https://doi.org/10.1016/j.neuropharm.2013.04.026

Koshland JR., D.E., 1959. Enzyme flexibility and enzyme action. J. Cell. Comp. Physiol. 54, 245–258. https://doi.org/10.1002/jcp.1030540420

Krishnamurthy, H., Gouaux, E., 2012. X-ray structures of LeuT in substrate-free outward-open and apo inward-open states. Nature 481, 469–474. https://doi.org/10.1038/nature10737

Kristensen, A.S., Andersen, J., Jørgensen, T.N., Sørensen, L., Eriksen, J., Loland, C.J., Strømgaard, K., Gether, U., 2011. SLC6 neurotransmitter transporters: structure, function, and regulation. Pharmacol. Rev. 63, 585–640. https://doi.org/10.1124/pr.108.000869

Krnjević, K., Schwartz, S., 1967. The action of γ-Aminobutyric acid on cortical neurones. Exp. Brain Res. 3, 320–336. https://doi.org/10.1007/BF00237558

Lindorff-Larsen, K., Piana, S., Palmo, K., Maragakis, P., Klepeis, J.L., Dror, R.O., Shaw, D.E., 2010. Improved side-chain torsion potentials for the Amber ff99SB protein force field. Proteins 78, 1950–1958. https://doi.org/10.1002/prot.22711

Mager, S., Naeve, J., Quick, M., Labarca, C., Davidson, N., Lester, H.A., 1993. Steady states, charge movements, and rates for a cloned GABA transporter expressed in Xenopus oocytes. Neuron 10, 177–188. https://doi.org/10.1016/0896-6273(93)90309-F

Merkle, P.S., Gotfryd, K., Cuendet, M.A., Leth-Espensen, K.Z., Gether, U., Loland, C.J., Rand, K.D., 2018. Substrate-modulated unwinding of transmembrane helices in the NSS transporter LeuT. Sci. Adv. 4, eaar6179. https://doi.org/10.1126/sciadv.aar6179

Michaud-Agrawal, N., Denning, E.J., Woolf, T.B., Beckstein, O., 2011. MDAnalysis: A toolkit for the analysis of molecular dynamics simulations. J. Comput. Chem. 32, 2319–2327. https://doi.org/10.1002/jcc.21787

Molgedey, L., Schuster, H.G., 1994. Separation of a mixture of independent signals using time delayed correlations. Phys. Rev. Lett. 72, 3634–3637. https://doi.org/10.1103/PhysRevLett.72.3634

Monod, J., Wyman, J., Changeux, J.-P., 1965. On the nature of allosteric transitions: A plausible model. J. Mol. Biol. 12, 88–118. https://doi.org/10.1016/S0022-2836(65)80285-6

Monticelli, L., Kandasamy, S.K., Periole, X., Larson, R.G., Tieleman, D.P., Marrink, S.-J., 2008. The MARTINI Coarse-Grained Force Field: Extension to Proteins. J. Chem. Theory Comput. 4, 819–834. https://doi.org/10.1021/ct700324x

Motiwala, Z., Aduri, N.G., Shaye, H., Han, G.W., Lam, J.H., Katritch, V., Cherezov, V., Gati, C., 2022. Structural basis of GABA reuptake inhibition. Nature 606, 820–826. https://doi.org/10.1038/s41586-022-04814-x

Naritomi, Y., Fuchigami, S., 2013. Slow dynamics of a protein backbone in molecular dynamics simulation revealed by time-structure based independent component analysis. J. Chem. Phys. 139, 215102. https://doi.org/10.1063/1.4834695

Nayak, S.R., Joseph, D., Höfner, G., Dakua, A., Athreya, A., Wanner, K.T., Kanner, B.I., Penmatsa, A., 2023. Cryo-EM structure of GABA transporter 1 reveals substrate recognition and transport mechanism. Nat. Struct. Mol. Biol. 1–10. https://doi.org/10.1038/s41594-023-01011-w

Parrinello, M., Rahman, A., 1981. Polymorphic transitions in single crystals: A new molecular dynamics method. J. Appl. Phys. 52, 7182–7190. https://doi.org/10.1063/1.328693

Penmatsa, A., Wang, K.H., Gouaux, E., 2013. X-ray structure of dopamine transporter elucidates antidepressant mechanism. Nature 503, 85–90. https://doi.org/10.1038/nature12533

Radian, R., Kanner, B.I., 1983. Stoichiometry of sodium- and chloride-coupled .gamma.-aminobutyric acid transport by synaptic plasma membrane vesicles isolated from rat brain. Biochemistry 22, 1236–1241. https://doi.org/10.1021/bi00274a038

Scherer, M.K., Trendelkamp-Schroer, B., Paul, F., Pérez-Hernández, G., Hoffmann, M., Plattner, N., Wehmeyer, C., Prinz, J.-H., Noé, F., 2015. PyEMMA 2: A Software Package for Estimation, Validation, and Analysis of Markov Models. J. Chem. Theory Comput. 11, 5525–5542. https://doi.org/10.1021/acs.jctc.5b00743

Schicker, K., Uzelac, Z., Gesmonde, J., Bulling, S., Stockner, T., Freissmuth, M., Boehm, S., Rudnick, G., Sitte, H.H., Sandtner, W., 2012. Unifying concept of serotonin transporter-associated currents. J. Biol. Chem. 287, 438–445. https://doi.org/10.1074/jbc.M111.304261

Schousboe, A., Madsen, K.K., 2017. Delineation of the Role of Astroglial GABA Transporters in Seizure Control. Neurochem. Res. 42, 2019–2023. https://doi.org/10.1007/s11064-017-2188-x

Schousboe, A., Sarup, A., Larsson, O.M., White, H.S., 2004. GABA transporters as drug targets for modulation of GABAergic activity. Biochem. Pharmacol., Six Decades of GABA 68, 1557–1563. https://doi.org/10.1016/j.bcp.2004.06.041

Schrödinger, LLC, Warren DeLano, 2020. Pymol.

Singh, S.K., Piscitelli, C.L., Yamashita, A., Gouaux, E., 2008. A Competitive Inhibitor Traps LeuT in an Open-to-Out Conformation. Science 322, 1655–1661. https://doi.org/10.1126/science.1166777

Sohail, A., Jayaraman, K., Venkatesan, S., Gotfryd, K., Daerr, M., Gether, U., Loland, C.J., Wanner, K.T., Freissmuth, M., Sitte, H.H., Sandtner, W., Stockner, T., 2016. The Environment Shapes the Inner Vestibule of LeuT. PLOS Comput. Biol. 12, e1005197. https://doi.org/10.1371/journal.pcbi.1005197

Szöllősi, D., Stockner, T., 2022. Sodium Binding Stabilizes the Outward-Open State of SERT by Limiting Bundle Domain Motions. Cells 11, 255. https://doi.org/10.3390/cells11020255

Szöllősi, D., Stockner, T., 2021. Investigating the Mechanism of Sodium Binding to SERT Using Direct Simulations. Front. Cell. Neurosci. 15.

Tavoulari, S., Margheritis, E., Nagarajan, A., DeWitt, D.C., Zhang, Y.-W., Rosado, E., Ravera, S., Rhoades, E., Forrest, L.R., Rudnick, G., 2016. Two Na+ Sites Control Conformational Change in a Neurotransmitter Transporter Homolog*. J. Biol. Chem. 291, 1456–1471. https://doi.org/10.1074/jbc.M115.692012

van Meer, G., 1998. Lipids of the Golgi membrane. Trends Cell Biol. 8, 29–33. https://doi.org/10.1016/s0962-8924(97)01196-3

Varadi, M., Anyango, S., Deshpande, M., Nair, S., Natassia, C., Yordanova, G., Yuan, D., Stroe, O., Wood, G., Laydon, A., Žídek, A., Green, T., Tunyasuvunakool, K., Petersen, S., Jumper, J., Clancy, E., Green, R., Vora, A., Lutfi, M., Figurnov, M., Cowie, A., Hobbs, N., Kohli, P., Kleywegt, G., Birney, E., Hassabis, D., Velankar, S., 2022. AlphaFold Protein Structure Database: massively expanding the structural coverage of protein-sequence space with high-accuracy models. Nucleic Acids Res. 50, D439–D444. https://doi.org/10.1093/nar/gkab1061

Wassenaar, T.A., Ingólfsson, H.I., Böckmann, R.A., Tieleman, D.P., Marrink, S.J., 2015. Computational Lipidomics with insane: A Versatile Tool for Generating Custom Membranes for Molecular Simulations. J. Chem. Theory Comput. 11, 2144–2155. https://doi.org/10.1021/acs.jctc.5b00209

Wolf, M.G., Hoefling, M., Aponte-Santamaría, C., Grubmüller, H., Groenhof, G., 2010. g_membed: Efficient insertion of a membrane protein into an equilibrated lipid bilayer with minimal perturbation. J. Comput. Chem. 31, 2169–2174. https://doi.org/10.1002/jcc.21507

Yamashita, A., Singh, S.K., Kawate, T., Jin, Y., Gouaux, E., 2005. Crystal structure of a bacterial homologue of Na+/Cl--dependent neurotransmitter transporters. Nature 437, 215–223. https://doi.org/10.1038/nature03978

Yang, D., Gouaux, E., 2021. Illumination of serotonin transporter mechanism and role of the allosteric site. Sci. Adv. 7, eabl3857. https://doi.org/10.1126/sciadv.abl3857

Zhang, Y.-W., Tavoulari, S., Sinning, S., Aleksandrova, A.A., Forrest, L.R., Rudnick, G., 2018. Structural elements required for coupling ion and substrate transport in the neurotransmitter transporter homolog LeuT. Proc. Natl. Acad. Sci. 115, E8854–E8862. https://doi.org/10.1073/pnas.1716870115

Zhao, Y., Terry, D.S., Shi, L., Quick, M., Weinstein, H., Blanchard, S.C., Javitch, J.A., 2011. Substrate-modulated gating dynamics in a Na+-coupled neurotransmitter transporter homologue. Nature 474, 109–113. https://doi.org/10.1038/nature09971

Zhu, A., Huang, J., Kong, F., Tan, J., Lei, J., Yuan, Y., Yan, C., 2023. Molecular basis for substrate recognition and transport of human GABA transporter GAT1. Nat. Struct. Mol. Biol. 1–11. https://doi.org/10.1038/s41594-023-00983-z

Zomot, E., Bendahan, A., Quick, M., Zhao, Y., Javitch, J.A., Kanner, B.I., 2007. Mechanism of chloride interaction with neurotransmitter:sodium symporters. Nature 449, 726–730. https://doi.org/10.1038/nature06133

Zwanzig, R., 1983. From classical dynamics to continuous time random walks. J. Stat. Phys. 30, 255–262. https://doi.org/10.1007/BF01012300

Supplementary Information

Title:

Interaction of GAT1 with sodium ions: from efficient recruitment to stabilisation of substrate and conformation

Authors:

Erika Lazzarin[1$], Ralph Gradisch[1$], Sophie M.C. Skopec[1], Leticia Alves da Silva[1], Dániel Szöllősi[1,2], Julian Maier[1], Sonja Sucic[1], Baruch I. Kanner[3], Harald H. Sitte[1,4,5], Thomas Stockner[1#]

Affiliations:

[1] Centre for Physiology and Pharmacology, Institute of Pharmacology, Medical University of Vienna, Waehrigerstr. 13A, 1090 Vienna, Austria

[2] Department of Theoretical and Computational Biophysics, Max Planck Institute for Multidisciplinary Sciences, Am Fassberg 11, 37077 Göttingen, Germany

[3] Department of Biochemistry and Molecular Biology, Institute for Medical Research Israel-Canada, Hebrew University, Hadassah Medical School, Jerusalem 91120, Israel

[4] Center for Addiction Research and Science-AddRess, Medical University Vienna, Waehringer Strasse 13A, 1090, Vienna, Austria

[5] Hourani Center for Applied Scientific Research, Al-Ahliyya Amman University, Amman, Jordan

#corresponding author

Thomas Stockner; email: thomas.stockner@meduniwien.ac.at

$ Shared first authors

These authors contributed evenly to the manuscript.

Contents:

Supplementary Figures, Molecular dynamics production parameters

Supplementary Figure 1. The compactness of the binding sites.

The compactness was quantified by first determining the center of mass (CoM) between coordinating atoms of the sodium binding sites NA1 and NA2, respectively, and by measuring the average distances between the CoM and the coordinating atoms. **(a)** Represents the time evolution of NA1 and NA2 compactness, where the time point of sodium entering NA1, NA2, or the temporary site (TMP) is indicated by a vertical line, colored according to the legend.

a

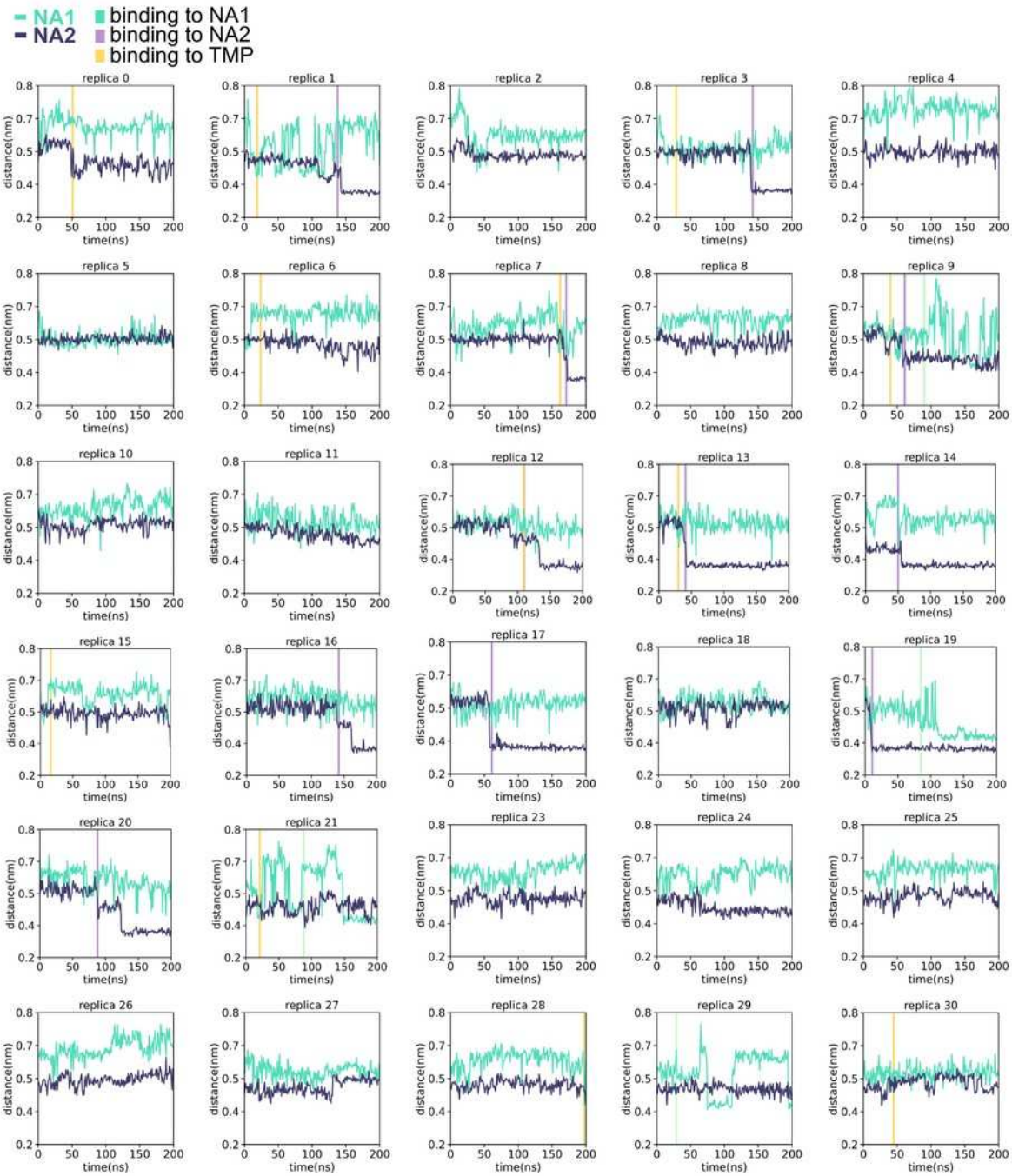

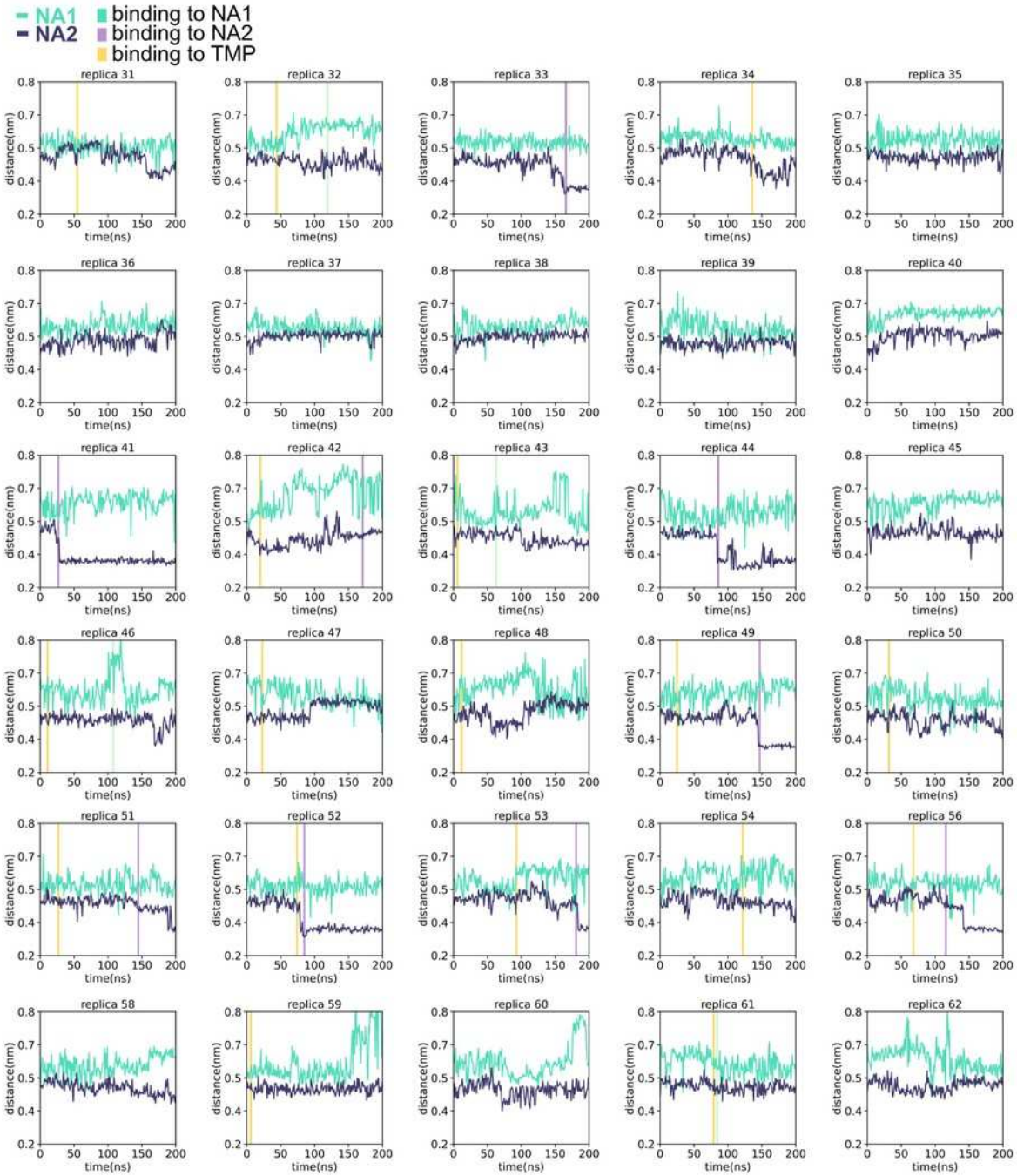

Supplementary Figure 2. Principal components analysis of NA1.

We concatenated the trajectories and conducted a PCA analysis. The covariance matrix was calculated using all trajectories, focusing on the atoms of the transmembrane helices (49:75, 64:76, 80:109, 121:155, 212:230, 282:309, 316:348,321345, 377:411, 420:439). The transmembrane helices C-alpha atoms were used as the fitting group. Subsequently, we divided the trajectories into two groups based on Na1 or Na2 binding and projected them onto the principal components previously calculated. these are shown as scatterplots in **(a,b)**, where the pink triangle corresponds to the NaCl-bound protein conformation.

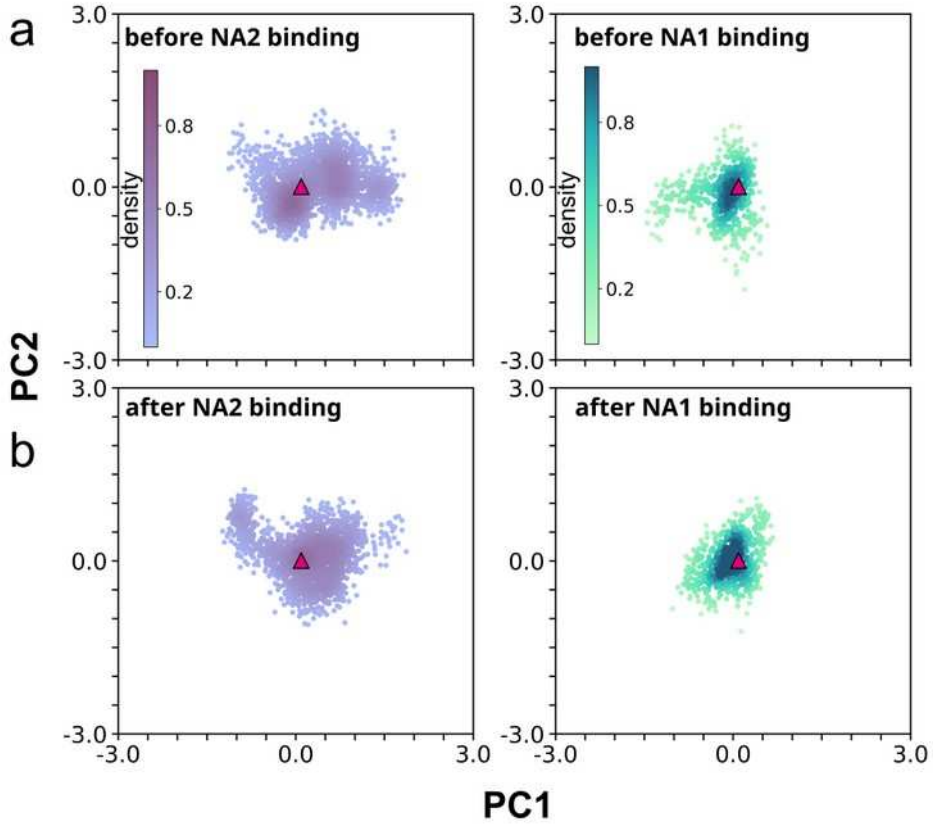

Supplementary Figure 3. Markovian behavior validation.

(a) show the result of the Chapman-Kolmogorov (CK) test using a lag time equal to 25 ns and assuming four macrostates. The predicted values obtained from our MSMs are shown by the solid lines while the estimated values for longer lag time are shown by the dashed traces. The superposition of predicted and estimated values indicates that the MSM assures the Markovian behavior. (b) displays the time traces of the relation between the lag time and the implied timescales (or relaxation time) associated with the ten slowest processes, with the top blue trace indicating the slowest process. The solid lines refer to the maximum likelihood result and the dashed lines show the ensemble mean computed with Bayesian sampling procedure. The black line with the grey area indicates the timescale threshold where the MSM cannot resolve processes. In both panels, the non-grey areas indicate 95% confidence intervals computed using the Bayesian sampling procedure mentioned above.

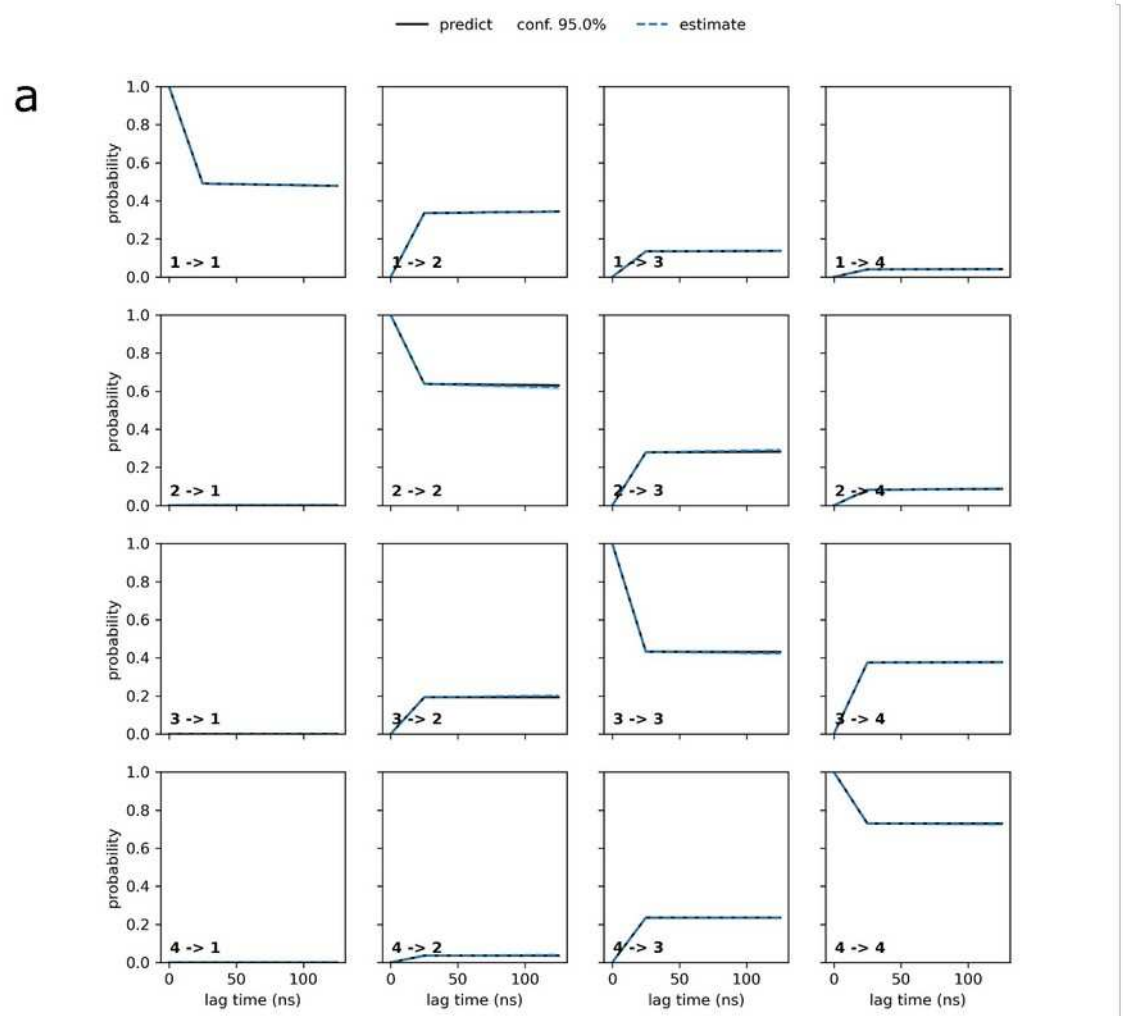

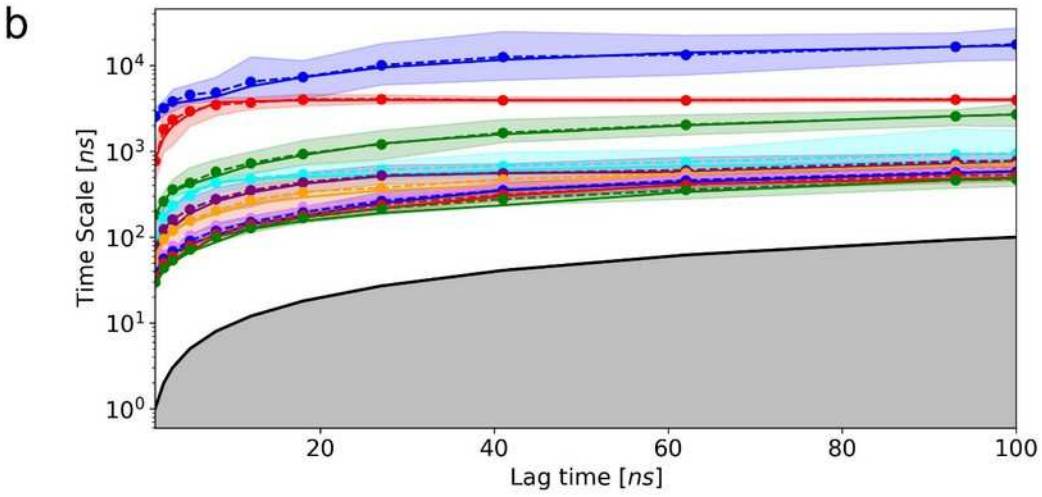

MDP file

```
;
;     File 'mdout.mdp' was generated
;     By user: stockner (1000)
;     On host: pha60
;     At date: Thu Oct 29 14:59:30 2015
;

; VARIOUS PREPROCESSING OPTIONS
; Preprocessor information: use cpp syntax.
; e.g.: -I/home/joe/doe -I/home/mary/roe
;include                  =
;  e.g.: -DPOSRES -DFLEXIBLE (note these variable names are case
sensitive)
;define                   = -DPOSRES

; RUN CONTROL PARAMETERS
integrator               = md
; Start time and timestep in ps
tinit                    = 0
dt                       = 0.002
nsteps                   = 500000000 ;1000 ns
; For exact run continuation or redoing part of a run
init_step                = 0
; Part index is updated automatically on checkpointing (keeps files
separate)
simulation_part          = 1
; mode for center of mass motion removal
comm-mode                = linear
; number of steps for center of mass motion removal
nstcomm                  = 100
; group(s) for center of mass motion removal
comm-grps                = ProtLigIon membrane Water_and_ions

; LANGEVIN DYNAMICS OPTIONS
; Friction coefficient (amu/ps) and random seed
bd-fric                  = 0
ld-seed                  = 1993

; ENERGY MINIMIZATION OPTIONS
; Force tolerance and initial step-size
emtol                    = 1000
emstep                   = 0.0001
; Max number of iterations in relax-shells
```

```
niter                    = 20
; Step size (ps^2) for minimization of flexible constraints
fcstep                   = 0.001
; Frequency of steepest descents steps when doing CG
nstcgsteep               = 50
nbfgscorr                = 100

; TEST PARTICLE INSERTION OPTIONS
rtpi                     = 0.05

; OUTPUT CONTROL OPTIONS
; Output frequency for coords (x), velocities (v) and forces (f)
nstxout                  = 5000 ; 10 ps
nstvout                  =
nstfout                  = 0
; Output frequency for energies to log file and energy file
nstlog                   = 1000
nstcalcenergy            = 100
nstenergy                = 1000
; Output frequency and precision for .xtc file
nstxout-compressed       = 0
compressed-x-precision   = 1000
; This selects the subset of atoms for the compressed
; trajectory file. You can select multiple groups. By
; default, all atoms will be written.
compressed-x-grps        =
; Selection of energy groups
energygrps               =

; NEIGHBORSEARCHING PARAMETERS
; cut-off scheme (Verlet: particle based cut-offs, group: using
charge groups)
cutoff-scheme            = Verlet
; nblist update frequency
nstlist                  = 50
; ns algorithm (simple or grid)
ns-type                  = Grid
; Periodic boundary conditions: xyz, no, xy
pbc                      = xyz
periodic_molecules       = no
; Allowed energy error due to the Verlet buffer in kJ/mol/ps per
atom,
; a value of -1 means: use rlist
verlet-buffer-tolerance  = 0.005
; nblist cut-off
rlist                    = 0.9
```

```
; long-range cut-off for switched potentials
rlistlong                = -1
nstcalclr                = -1

; OPTIONS FOR ELECTROSTATICS AND VDW
; Method for doing electrostatics
coulombtype              = PME
coulomb-modifier         = Potential-shift-Verlet
rcoulomb-switch          =
rcoulomb                 = 0.9
; Relative dielectric constant for the medium and the reaction field
epsilon_r                = 1.0
epsilon_rf               = 1
; Method for doing Van der Waals
vdw-type                 = Cut-off
vdw-modifier             = Potential-shift-Verlet
; cut-off lengths
rvdw-switch              =
rvdw                     = 0.9
; Apply long range dispersion corrections for Energy and Pressure
DispCorr                 = EnerPres
; Extension of the potential lookup tables beyond the cut-off
table-extension          = 1
; Separate tables between energy group pairs
energygrp-table          =
; Spacing for the PME/PPPM FFT grid
fourierspacing           = 0.12
; FFT grid size, when a value is 0 fourierspacing will be used
fourier_nx               = 0
fourier_ny               = 0
fourier_nz               = 0
; EWALD/PME/PPPM parameters
pme_order                = 4
ewald_rtol               = 1e-05
ewald-rtol-lj            = 0.001
lj-pme-comb-rule         = Geometric
ewald_geometry           = 3d
epsilon_surface          = 0

; IMPLICIT SOLVENT ALGORITHM
implicit_solvent         = No

; GENERALIZED BORN ELECTROSTATICS
; Algorithm for calculating Born radii
gb-algorithm             = Still
; Frequency of calculating the Born radii inside rlist
```

```
nstgbradii              = 1
; Cutoff for Born radii calculation; the contribution from atoms
; between rlist and rgbradii is updated every nstlist steps
rgbradii                = 1
; Dielectric coefficient of the implicit solvent
gb-epsilon-solvent      = 80
; Salt concentration in M for Generalized Born models
gb-saltconc             = 0
; Scaling factors used in the OBC GB model. Default values are
OBC(II)
gb-obc-alpha            = 1
gb-obc-beta             = 0.8
gb-obc-gamma            = 4.85
gb-dielectric-offset    = 0.009
sa-algorithm            = Ace-approximation
; Surface tension (kJ/mol/nm^2) for the SA (nonpolar surface) part
of GBSA
; The value -1 will set default value for Still/HCT/OBC GB-models.
sa-surface-tension      = -1

; OPTIONS FOR WEAK COUPLING ALGORITHMS
; Temperature coupling
tcoupl                  = v-rescale
nsttcouple              = -1
nh-chain-length         = 10
print-nose-hoover-chain-variables = no
; Groups to couple separately
tc-grps                 = ProtLigIon membrane Water_and_ions
; Time constant (ps) and reference temperature (K)
tau-t                   = 0.5   0.5   0.5
ref-t                   = 310   310   310
; pressure coupling
Pcoupl                   = Parrinello-Rahman ; Berendsen for EM and
equilibration;Parrinello-Rahman for production
Pcoupltype              = Semiisotropic
nstpcouple              = -1
; Time constant (ps), compressibility (1/bar) and reference P (bar)
tau-p                    = 20.1       ; Use 5 for Berendsen; 20 for
Parrinello-Rahman;
compressibility         = 4.5e-05   4.5e-05
ref-p                   = 1.0       1.0
; Scaling of reference coordinates, No, All or COM
refcoord_scaling        = All


; SIMULATED ANNEALING
```

```
; Type of annealing for each temperature group (no/single/periodic)
annealing                = no
; Number of time points to use for specifying annealing in each
group
annealing-npoints        =
; List of times at the annealing points for each group
annealing-time           =
; Temp. at each annealing point, for each group.
annealing-temp           =

; GENERATE VELOCITIES FOR STARTUP RUN
gen-vel                  = no
gen-temp                 = 310.0
gen-seed                 = -1

; OPTIONS FOR BONDS
constraints              = h-bonds
; Type of constraint algorithm
constraint-algorithm     = lincs
; Do not constrain the start configuration
continuation             = no
; Use successive overrelaxation to reduce the number of shake
iterations
Shake-SOR                = yes
; Relative tolerance of shake
shake-tol                = 0.0001
; Highest order in the expansion of the constraint coupling matrix
lincs-order              = 4
; Number of iterations in the final step of LINCS. 1 is fine for
; normal simulations, but use 2 to conserve energy in NVE runs.
; For energy minimization with constraints it should be 4 to 8.
lincs-iter               = 2
; Lincs will write a warning to the stderr if in one step a bond
; rotates over more degrees than
lincs-warnangle          = 30
; Convert harmonic bonds to morse potentials
morse                    = no

; ENERGY GROUP EXCLUSIONS
; Pairs of energy groups for which all non-bonded interactions are
excluded
energygrp-excl           =

; WALLS
; Number of walls, type, atom types, densities and box-z scale
factor for Ewald
```

```
nwall                    = 0
wall_type                = 9-3
wall_r_linpot            = -1
wall-atomtype            =
wall-density             =
wall_ewald_zfac          = 3

; COM PULLING
; Pull type: no, umbrella, constraint or constant-force
pull                     = no

; ENFORCED ROTATION
; Enforced rotation: No or Yes
rotation                 = no

; Group to display and/or manipulate in interactive MD session
IMD-group                =

; NMR refinement stuff
; Distance restraints type: No, Simple or Ensemble
disre                    = No
; Force weighting of pairs in one distance restraint: Conservative
or Equal
disre-weighting          = Conservative
; Use sqrt of the time averaged times the instantaneous violation
disre-mixed              = no
disre-fc                 = 100
disre-tau                = 0
; Output frequency for pair distances to energy file
nstdisreout              = 5000
; Orientation restraints: No or Yes
orire                    = no
; Orientation restraints force constant and tau for time averaging
orire-fc                 = 0
orire-tau                = 0
orire-fitgrp             =
; Output frequency for trace(SD) and S to energy file
nstorireout              = 100

; Free energy variables
free-energy              = no
couple-moltype           =
couple-lambda0           = vdw-q
couple-lambda1           = vdw-q
couple-intramol          = no
init-lambda              = 0
```

```
init-lambda-state        = -1
delta-lambda             = 0
nstdhdl                  = 50
fep-lambdas              =
mass-lambdas             =
coul-lambdas             =
vdw-lambdas              =
bonded-lambdas           =
restraint-lambdas        =
temperature-lambdas      =
calc-lambda-neighbors    = 1
init-lambda-weights      =
dhdl-print-energy        = no
sc-alpha                 = 0
sc-power                 = 1
sc-r-power               = 6
sc-sigma                 = 0.3
sc-coul                  = no
separate-dhdl-file       = yes
dhdl-derivatives         = yes
dh_hist_size             = 0
dh_hist_spacing          = 0.1

; Non-equilibrium MD stuff
acc-grps                 =
accelerate               =
freezegrps               =
freezedim                =
cos-acceleration         = 0
deform                   =

; simulated tempering variables
simulated-tempering      = no
simulated-tempering-scaling = geometric
sim-temp-low             = 300
sim-temp-high            = 300

; Electric fields
; Format is number of terms (int) and for all terms an amplitude
(real)
; and a phase angle (real)
E-x                      =
; Time dependent (pulsed) electric field. Format is omega, time for
pulse
; peak, and sigma (width) for pulse. Sigma = 0 removes pulse,
leaving
```

```
; the field to be a cosine function.
E-xt                    =
E-y                     =
E-yt                    =
E-z                     =
E-zt                    =

; Ion/water position swapping for computational electrophysiology
setups
; Swap positions along direction: no, X, Y, Z
swapcoords              = no

; AdResS parameters
adress                  = no

; User defined thingies
user1-grps              =
user2-grps              =
userint1                = 0
userint2                = 0
userint3                = 0
userint4                = 0
userreal1               = 0
userreal2               = 0
userreal3               = 0
userreal4               = 0
```